Journal of Sustainable Construction Materials and Technologies

Volume 11 | Issue 2 Article 9

Optimizing Graphene Oxide in Self-Compacting Concrete: A Sustainable Nano-Material Strategy for Enhanced Durability and Structural Performance

Mohammed Shakeebulla Khan

Department of Civil Engineering, Govt. SKSJ Technological Institute, Visvesvaraya Technological University, Belagavi-590 018, Karnataka, India AND Department of Civil Engineering, St. John College of Engineering and Management, Palghar, Mumbai, Maharashtra 401404, India, shakeeb.ulla@gmail.com

Vijaya G. S

Department of Civil Engineering, Govt. SKSJ Technological Institute, Visvesvaraya Technological University, Belagavi-590 018, Karnataka, India

JOURNAL OF SUSTAINABLE CONSTRUCTION MATERIALS AND TECHNOLOGIES 2026;11:338–368

RESEARCH ARTICLE

Optimizing Graphene Oxide in Self-Compacting Concrete: A Sustainable Nano-Material Strategy for Enhanced Durability and Structural Performance

Mohammed Shakeebulla Khan [a,b,*], **Vijaya G. S** [a]

[a] Department of Civil Engineering, Govt. SKSJ Technological Institute, Visvesvaraya Technological University, Belagavi-590 018, Karnataka, India
[b] Department of Civil Engineering, St. John College of Engineering and Management, Palghar, Mumbai, Maharashtra 401404, India

ABSTRACT

In order to reduce the environmental impact of the constructed world, advanced and sustainable construction materials are needed. This work is a summary of the comprehensive study on a novel self-compacting concrete with nano-engineered material (graphene oxide) modified self-compacting concrete (GO-SCC). The optimum dosage of GO was determined using Taguchi method, Analysis of Variance (ANOVA) and Response Surface Methodology (RSM) multi-objective statistical optimization method, and was found to be 0.10% by weight of cement (bwoc). This dosage of 0.10% GO led to the overall desirability score of 0.87, which confirmed that this was the optimum dosage for six response variables simultaneously for the global level. It helps to overcome the workability-strength-durability challenge. which has been problematic in the production of nano-modified concrete in a way that maintains the self-compactability (EFNARC compliant) required in the concrete and enhances its performance. The optimized composite has highest improvement in mechanical strength, which is 48 to 50%, and also has highest improvement in Durability based on 72% reduction in chloride penetrability in RCPT (3500 to 980 Coulombs) and 58.4% reduction in water sorptivity. The results are higher than in the previous GO-SCC studies. Three synergistic effects of nucleation acceleration, nano-filler pore densification, and crack-bridging in the microstructural analysis have been identified as a significant link, which makes GO a nano-reinforcement and nucleus that raises the density and refinement of the cementitious matrix. The employment of fly ash as supplementary cementing material (as SRC) supports the idea of circular economy and waste valorization since it diverts around 97 kg/m^3 of the industrial by-product from landfill and cuts the embodied CO_2 by 60-70 kg/m^3.

Keywords: Sustainable construction materials, Graphene oxide, Self-compacting concrete, Statistical optimization, Durability, Circular economy, Nano-reinforcement

1. Introduction

1.1. The macro context, built environment, energy and sustainability

A major key focus of this course is the macro context, Built Environment, Energy and Sustainability. The built environment consumes almost 40% of the energy used on a global scale, which is emitted as GHGs [1, 2]. Much of this effect is reflected in the construction materials and occurs during the life of the building in the maintenance, repair and replacement phases [2]. In this regard, improving the durability and lifespan of construction materials is one of the most important ways of meeting the sustainability goals in the global agenda stated in the United Nations Sustainable Development Goals (SDGs) [3]. In this context, the use of concrete is the largest of

Received 16 December 2025; revised 17 May 2026; accepted 5 June 2026.
Available online 17 June 2026

* Corresponding author.
E-mail address: shakeeb.ulla@gmail.com;shakeebullak@sjcem.edu.in (M. S. Khan).

https://doi.org/10.29187/2458-973X.1225

man-made materials, offering a big opportunity for innovation. Portland cement production is responsible for around 8% of global anthropogenic CO_2 emissions, and a paradigm shift is needed in the materials industry to move to high-performance materials with low embodied carbon and lifecycle maintenance costs [4].

1.2. Self-compacting concrete and its inherent challenges

Self-Compacting Concrete (SCC) is another revolutionary development in concrete technology developed to flow and compact under their own weight, which eliminates the need for mechanical vibration in the construction process [5–7]. This is a superior performance in the fresh state, which reduces the risk of construction defects, and assures a high in-place density and homogeneity, essential for long-term durability. A recognizable conflict between these characteristics exists, however, because the high fluidity obtained from SCC is frequently obtained at the expense of higher paste volume, and chemical admixtures which may result in different properties compared to concrete produced by conventional vibration. This intrinsic constraint represents a limitation for the use of SCC in the field of sustainable and long-life infrastructures, where excellent constructability and high performance are essential [8–10].

1.3. The role of durability and the promise of nanotechnology

The service-life for concrete structures is defined by its durability, which is strongly related to the ability of the concrete to resist the passage of harmful fluids and ions, and which is primarily determined by the transport properties (such as chloride diffusivity) of the concrete. Graphene Oxide (GO), a 2D carbon based nanomaterial with a layer of oxygen functional groups (hydroxyl, epoxide, carboxyl) has received much attention as the best nano-reinforcement [11, 12]. It works in the cementitious matrices by three main mechanisms: (i) as a nucleation site for the formation of C-S-H gel, promoting cementitious hydration and improving the microstructure (ii) as a nano-filler, providing densification of the matrix and reducing matrix permeability and (iii) as a microcrack bridging effect, increasing the energy required to break the matrix and the mechanical strength. GO directly supports SDG 9 (Industry, Innovation and Infrastructure), SDG 11 (Sustainable Cities) and SDG 13 (Climate Action) through the creation of sustainable and low-maintenance infrastructure, using less energy in its life cycle [13].

1.4. Identifying the critical research gap

Although impressive success has been achieved with SCC in conventional concrete, the incorporation into the more complicated, admixture-rich concrete system of SCC has been studied significantly less and is fundamentally limited by conflicting requirements [14]. The high specific surface area of GO absorbs water and leads to a rise in the viscosity, which is the most important characteristic for SCC. One of the key research challenges is the lack of an effective, multi-criteria optimization model that can determine the optimum dosage that is best for both workability, strength and durability. Current studies only evaluate limited doses of GO ($\leq$ 0.05%) or examine single properties without proper statistical verification.

1.5. Describing our novel contribution and objective

This research is designed in a systematic approach to tackle the identified research gap by developing a comprehensive optimization framework for the incorporation of graphene oxide in self-compacting concrete, using a statistically driven approach. The most important innovation is the development of the first Taguchi-RSM-ANOVA an integrated optimization approach for GO-SCC over the entire dosage range (0–0.12%) that provides a practical method for use without can be used without changing the standard mix designs. In addition, the use of Class F fly ash as 24 per cent replacement of cement directly contributes to the principles of circular economy and waste valorization as per SDG-9 (Industry, Innovation and Infrastructure), SDG-11 (Sustainable Cities and Communities) and SDG-13 (Climate Action), by diverting appx. 97 kg/m^3 of combustion by-product from landfills, and reducing the demand for clinker by appx. 24%, which lowers the embodied CO_2 by approximately 60 to 70 kg/m^3 as compared to a pure OPC mix.

2. Literature review

2.1. The sustainability imperative and durable concrete

Energy consumption and carbon emissions related to the built environment represent almost 40% of global energy consumption and carbon emissions [15]. Around 8% of anthropogenic CO_2 is emitted as a result of Portland cement production [16]. This has spurred the shift to more sustainable concrete

technologies that not only cut initial embodied carbon, but also improve durability to lower life-cycle energy use due to maintenance and reconstruction. The idea of designing for durability has now gained prominence as one of the key strategies in harmony with circular economy principles [16].

2.2. Self-compacting concrete: Evolution, principles, and challenges

SCC was developed in Japan in the late 1980s by Okamura and his colleagues, which was designed to flow under its own weight, fully filling the formwork and passing through congested reinforcement without mechanical vibration. The slump flow (filling ability), V-funnel or T_{50} time (viscosity) and L-box or J-ring (passing ability) are used to measure self-compactability. Although SCC has better properties in the fresh state and produces better in-place homogeneity, using more powder in the concrete mix and higher dosages of HRWRA can result in in-place properties of lower mechanical strength and transport characteristics, and higher hydration heat than the same concrete produced by conventional vibrated concrete [5, 14, 17, 18].

2.3. Graphene oxide as a premier nano-reinforcement

In this section, the role of graphene oxide as a leading nano-reinforcement material is discussed. From all nanomaterials (nano-silica, carbon nanotubes) Graphene Oxide (GO) has become one of the most promising nano-reinforcements for its unique combination of properties [19–23]. GO is obtained by the chemical oxidation of graphite through Hummers method. It is oxygen rich with functional groups (hydroxyl, epoxide, carbonyl, carboxyl) that give it a high level of hydrophilicity which result in good colloidal dispersion in water and also in the presence of many active sites for interaction with the hydration products of cement. GO surface is functionalized and this functional group provides greater efficacy in modifying the cement hydrate matrix as opposed to pristine graphene [24–26].

2.4. Mechanisms of enhancement

There are three well-known synergistic mechanisms responsible for the improvement of the properties of these cementitious systems when GO is added:

- **Nucleation Site Effect**: The functional groups containing oxygen found on the surfaces of GO act as ideal nucleation sites for the precipitation and early hydration of C-S-H gel, which results in a more refined and dense microstructure [27]
- **Filler Effect**: Being ultra-thin and planar (0.5–2 nm), GO is a nano-filler, which can fill the nano-pores of the C-S-H gel and diminish the interconnected capillary pores (>50 nm) which are the major site for fluid and ion transport [28–30].
- **Crack-Bridging Effect: 2D** sheets with high aspect ratio and high intrinsic tensile strength ($\sim$100-130 GPa) can bridge the micro-cracks under stress, requiring more energy to move the cracks and thus providing a higher level of fracture toughness [31].

2.5. Performance evidence in concrete systems

The compressive strength enhancement is reported as 20-50% for conventional concrete with low dosage of GO (0.01-0.06% bwoc) in several studies [32]. Reductions greater than 50% in RCPT have been reported [33] and significant declines in the water sorptivity have been reported as well [34]. In the case of SCC, Tufail et al. [14] achieved up to 22% improvement in the case of the use of graphite nano/micro platelets and Khed et al. [35] observed an improvement of $\sim$30% in compressive strength with GO in fly ash SCC. In the current study these benchmarks are systematically surpassed.

2.6. The unresolved challenge: GO in SCC, and the research gap

Although GO has been demonstrated to be beneficial for conventional concrete, the addition of GO into SCC admixture system is challenging. Past research shows that the approach has been fragmentary and includes the following: (i) limited dosage testing ($\leq$ 0.05% bwoc) which is not sufficient to reveal the entire dosage-response curve with the agglomeration threshold; (ii) isolated analyses of properties where mechanical improvements have been reported but where multi-objective optimization is lacking; and (iii) no strong multi-objective optimization frameworks. The paper provides a detailed analysis, which clearly identifies that a practical dosage window for SCC which maintains sufficient self-compactability while achieving maximum mechanical strength and long-term durability has yet to be statistically validated and optimized using multiple criteria.

Table 1. Physical and chemical properties of OPC 53 cement.

Property / Test	Result	IS 12269:2013 Requirement
Specific Gravity	3.0	—
Standard Consistency (%)	27	—
Initial Setting Time (min)	170	≥ 30
Final Setting Time (min)	270	≤ 600
28-Day Compressive Strength (MPa)	41.5	≥ 53
Fineness (Blaine, m^2/kg)	284	≥ 225
CaO (%)	62.40	—
SiO_2 (%)	22.50	—
Al_2O_3 (%)	4.20	—
MgO (%)	2.10	≤ 6.0
SO_3 (%)	2.14	≤ 3.0
Loss on Ignition (%)	2.98	≤ 4.0

3. Materials and experimental methodology

3.1. Materials and properties

All the constituent materials were sourced from the local area and tested to ensure their conformity with Indian Standard (IS) codes. Ordinary Portland Cement (OPC) 53-grade (UltraTech Cement Ltd.) was used as the main binder, which is in accordance with IS 12269:2013 (specific gravity of 3.0 and Blaine fineness of 284 m^2/kg) as in Table 1. The fly ash used in the present study was Class F fly ash as per IS 3812 (Part 1):2013 with 45 μ residue of 12.5% by weight of specific gravity 2.10, which was used as supplementary cementitious material in the replacement of 24% of the cement as in Table 2. The fine aggregate used was manufactured sand (M-Sand) as per IS 383:2016 and coarse aggregate used was crushed granite aggregates with nominal size of 10 mm and 12 mm. Superplasticiser used: Polycarboxylate ether (PCE) high range water reducing admixture (BASF MasterGlenium SKY 8233). A commercially available aqueous suspension of Graphene Oxide (4 mg/ml concentration, Graphenea Inc.) with purity >95%, 3-5 layers, sheet size 1-5 μm, oxygen content ~45% was used as in Table 3 and Fig. 1 shows the Characterization of laboratory-synthesized Graphene Oxide.

3.2. Mixture proportions and experimental design

The control M40-grade SCC was prepared according to IS 10262:2019 [36] the EFNARC guidelines [37] and had a water to binder (w/b) ratio of 0.42, and a total powder content of 405 kg/m^3 Mix Proportions are shown in Table 4. The dosage of the superplasticizer was set at 1.0% which was determined by preliminary Marsh Cone tests (ASTM C939) [38] as described in Section 4.1. A one factor experimental design was used with GO dosage (% bwoc) at seven different levels: 0%, 0.02%, 0.04%, 0.06%, 0.08%, 0.10%, and 0.12%. The volume of GO suspension was substituted for an equal volume of water used in mixing for GO-incorporated mixes and the w/b ratio was the same for all mixes. The Taguchi method (L7 orthogonal array) [63, 64] was selected, and optimally designed to represent the full curve of the response for the performance from beneficial dispersion to detrimental agglomeration [39–42].

3.3. Advanced statistical optimization and analysis framework

İn this section, the paper states how to learn the use of advanced statistical optimization and analysis. To overcome the limitation of empirical analysis and provide a rigorous foundation for optimization based on the experimental data, the experimental data were analyzed comprehensively in multi-objective statistics, which consists of four integrated components: Some of the properties measured were used with the “Larger-is-Better” criterion ($S/N = -10\log_{10}(\Sigma(1/y^2)/n)$) for the strength properties and the “Smaller-is-Better” criterion (S/N =

Table 2. Chemical and physical characteristics of class-F fly ash.

Oxide	Percentage (%)	IS 3812 (Part 1):2013 Requirement
SiO_2	61.24	$SiO_2 + Al_2O_3 + Fe_2O_3 \geq 70\%$
Al_2O_3	25.00	—
Fe_2O_3	8.71	—
Total ($SiO_2 + Al_2O_3 + Fe_2O_3$)	94.95	≥ 70%
CaO	4.22	—
MGO	0.09	≤ 5.0%
SO_3	0.49	≤ 3.0%
Na_2O	0.09	≤ 1.5%
K_2O	0.66	—
Loss on Ignition (%)	1.50	≤ 5.0%
Physical Properties		
Specific Gravity	2.10	—
Fineness (45 μm residue, %)	12.5	≤ 34%

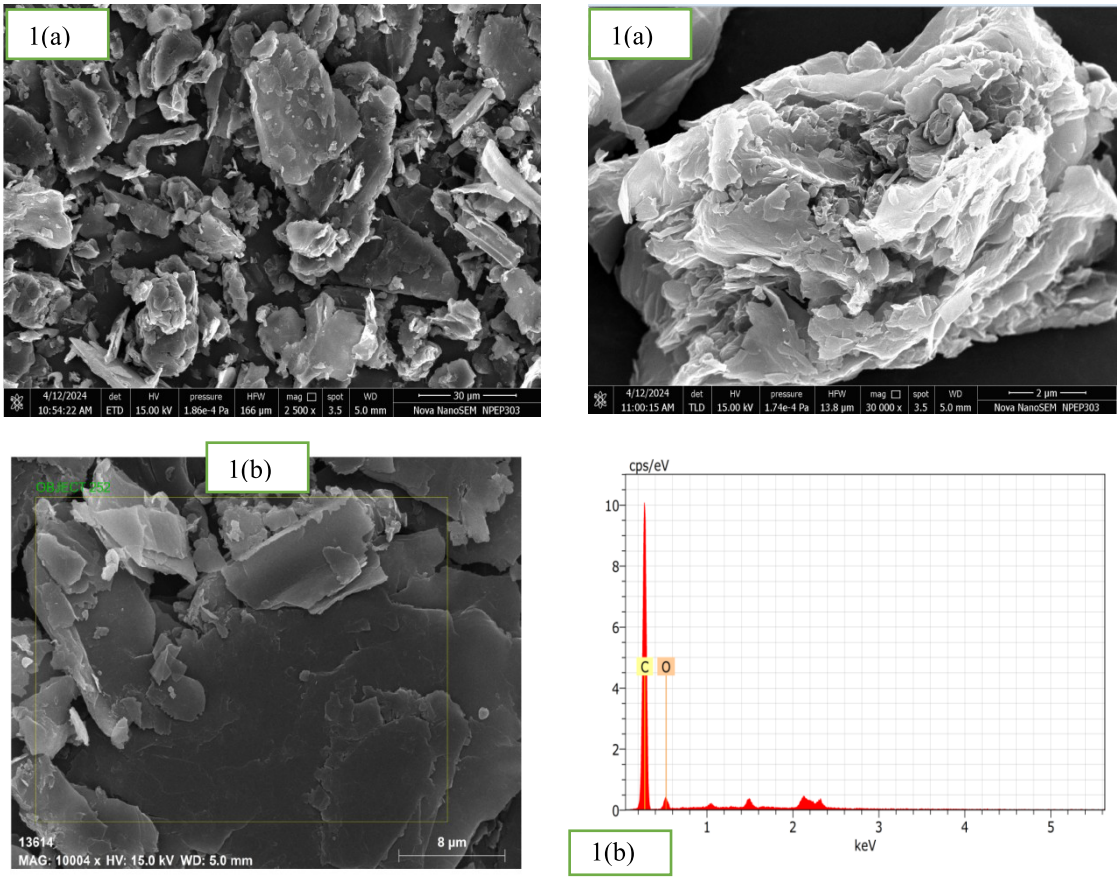

Fig. 1. Characterization of laboratory-synthesized Graphene Oxide: (a) FESEM image showing layered morphology; (b) EDS spectrum confirming successful oxidation with high carbon and oxygen content.

Table 3. Elemental and structural characteristics of graphene oxide.

Element / Property	Value	Method / Remark
Carbon (C)	49–56%	Major constituent (EDS)
Oxygen (O)	41–50%	Defines oxidation level (EDS)
Hydrogen (H)	0–1%	Trace
Number of Layers	3–5	FESEM
Sheet Size	1–5 μm	Lateral dimension (AFM)
Thickness	0.5–2 nm	AFM
Purity	>95%	EDS
Oxygen Content	~45%	Functional groups
Concentration	4 mg/ml	Aqueous suspension (Graphenea Inc.)

$-10\ \log_{110}(\Sigma y^2/n)$) for the RCPT, sorptivity, and flow times. This powerful analysis gives parameter levels that optimize performance while minimizing parameter-to-parameter variation, thus giving a value for process stability that is not dependent upon experimental noise.

- **Analysis of variance (ANOVA):** One-way ANOVA was used to examine the statistical significance of the GO factor (p-value < 0.05). ANOVA also quantified the contribution of the GO factor in terms of its percentage contribution (%PC), which is also used as a measure of its dominance in controlling the observed property variation. The F-statistic gave a quantitative evaluation of the ratio of the between group variance to within group variance [43, 44].
- **Response Surface Methodology (RSM):** Second-order polynomial models were developed describing functional relationships between GO dosage (X) and key mechanical properties. The coefficient of determination (R^2), adjusted R^2, and standard error of estimate were the measure of quality of fit. The model was validated by random distribution of the residuals with respect to the dosage levels and by leave-one-out cross validation (LOOC): predictions of the dosage levels not included in the training set, compressive strength within ±2.1%, sorptivity within ±1.8%, RCPT within ±3.5% [9, 45].
- **Desirability Function Approach**: Multi-objective simultaneous optimisation of six response variables slump flow (maximum, within EFNARC limit of 645–750 mm), 28-day

Table 4. Mix proportions for control SCC (per m^3).

Component	Quantity (kg/m^3)	Mass Ratio	Function
Cement (OPC 53)	308	1.00	Primary binder
Fly Ash (Class F)	97	0.32	Workability, durability, embodied carbon reduction
M-Sand (Zone II)	750	2.43	Fine aggregate
Coarse Aggregate 10 mm	834	2.71	Coarse aggregate
Coarse Aggregate 12 mm	358	1.16	Grading adjustment
Water	170 L	0.55	Hydration (replaced by GO suspension in GO mixes)
Superplasticizer (PCE)	4.05	0.013	Workability — fixed at 1.0% bwoc
w/b Ratio	0.42	—	Fixed across all mixes
Total Powder Content	405 kg/m^3	—	EFNARC requirement

compressive strength (maximum), split tensile strength (maximum), flexural strength (maximum), RCPT charge (minimum) and sorptivity (minimum) all response parameters being equally weighted. The target-based formulation was used to transform each individual desirability function to a dimensionless range (0 to 1), and the overall desirability (D) was calculated as the geometric mean of all individual desirability scores [46–48].

3.4. Specimen preparation, mixing process, and testing methods

Specimen Preparation, Mixing Process, and Testing Methods Homogeneous dispersion of GOs and steric stabilization by the addition of superplasticizer (SP) molecules to the GO sheets were ensured by the following carefully developed mixing Process: (i) sonicated GO suspension was diluted in the calculated volume of mixing water and sonicated again prior to the addition of the superplasticizer solution, to ensure maximum exfoliation without thermal degradation of functional groups, for 30 minutes at 60% amplitude while the mixing water was kept in ice bath (10s on, 5s off pulse cycle) [49–54]; (ii) the superplasticizer solution was added to the sonicated GO water and mixed for 5 minutes; (iii) coarse and fine aggregates were dry-mixed for 2 minutes; (iv) the binder (cement + fly ash) was added and mixed for 2 minutes, and (v) the allotted volume of the GO-SP-water solution was added and stirred for a further 5 minutes. All specimens were removed from the mould after 24 hours and water cured at 27±2°C till tested. The comprehensive testing program evaluated: fresh properties (slump flow, T_{50}, V-Funnel, L-Box, sieve segregation) per EFNARC and IS 1199; compressive strength (150 mm cubes) at 7, 14, 28, and 56 days per IS 516:2021 [55] split tensile strength (150×300 mm cylinders) at 28 days per IS 5816:2018, flexural strength (100×100×500 mm prisms) at 28 days per IS 516:2021, chloride ion penetration resistance (RCPT) per ASTM C1202 [56] and water sorptivity per ASTM C1585 [57]. At least three specimens per variable was used to make the data statistically significant.

4. Results and discussion:graphene oxide-modified self-compacting concrete: comprehensive performance analysis

4.1. Test results overview: Materials, dosages, and experimental design

4.1.1. Material characterization summary and property correlations

The choice and description of the constituent materials served as the platform on which all the following performance outcomes were developed. The material properties of the four main materials utilized in this study, OPC 53-grade cement, Class F fly ash, Graphene Oxide (GO) suspension and the polycarboxylate ether (PCE) superplasticizer are summarized in Table 5. To understand the composite behaviour of the GO-SCC, it is necessary to understand the properties of the individual materials, which provide different mechanisms contributing to the performance of the system under fresh, mechanical and durability considerations. The main cementitious matrix was provided by the OPC 53 grade cement (specific gravity 3.0, Blaine fineness 284 m^2/kg, 28-day strength 41.5 MPa). It has a standard consistency of 27% and initial setting time of 170 minutes which is in accordance with IS 12269:2013 [58] requirements and it was observed that SCC mixing was achieved with workability. The relatively lower 28-day strength (41.5 MPa compared to ≥ 53 MPa requirement) is due to the test procedure carried out at the material characterisation stage in the form of standard mortar cubes and is not a limitation on being able to design the mix to M40 SCC; a control mix was designed that achieved a final strength of 40.7 MPa. Specific gravity of Class F fly ash used was 2.10, with 45-um residue being 12.5% and 24% was replaced with cement by wt. It has a high pozzolanic reactivity (IS 3812 minimum is 70%, it has 94.95% combined ($SiO_2 + Al_2O_3 + Fe_2O_3$)) which is

Table 5. Comprehensive presentation of material properties and their significance for GO-SCC performance.

Material	Key Property	Value	Relevance to GO-SCC Performance
OPC 53	Specific Gravity	3.0	Controls paste volume and powder packing
OPC 53	Blaine Fineness	284 m^2/kg	Governs hydration rate and C-S-H nucleation sites
OPC 53	28d Mortar Strength	41.5 MPa	Baseline for cement quality assessment
Fly Ash	Specific Gravity	2.10	Lower than cement: reduces paste density, aids workability
Fly Ash	Pozzolanic Oxides	94.95%	High reactivity: secondary C-S-H, long-term durability
Fly Ash	CaO Content	4.22%	Class F: slow pozzolanic reaction, sustained strength gain
Fly Ash	Loss on Ignition	1.50%	Low carbon: maintains SP adsorption efficiency
GO Suspension	Oxygen Content	~45%	High functional group density: nucleation and dispersion
GO Suspension	Sheet Size (AFM)	1-5 um	Optimal for crack-bridging and nano-filler effect
GO Suspension	Layers (FESEM)	3-5	Multi-layer: balance of surface area and structural integrity
GO Suspension	Purity	> 95%	Consistent reactivity; minimal inert impurity
PCE-SP	Dosage	1.0% bwoc	Optimal: Marsh Cone confirmed saturation point

an important factor for long term strength development and durability. With a relatively low CaO content of 4.22%, its chemical characteristics are mostly siliceous, rather than cementitious, which promotes long-term pozzolanic reactions with the free calcium hydroxide (CH) produced by the cement's hydration. Low unburnt carbon content is indicated by the low LOI value of 1.50%, which is crucial to ensure the SP effectiveness and GO dispersion stability. The commercially purchased GO suspension (Graphenea Inc. (4mg/ml, purity >95%)) had oxygen content of ~45% indicating high level of oxidation and presence of surface functional groups (hydroxyl, epoxide, carboxyl). The 3-5 layered structure ([43, 59, 60]) and the size of the sheets of 1-5 um (AFM) are optimal for modification of the cementitious matrix as they are small enough to penetrate the inter-hydrate space resulting in useful nano-filler effect and large enough to effectively bridge the micro-cracks. The C:O ratio is around 49-56%:41-50%, showing that GO was moderately oxidized, which is essential for its stable aqueous suspension and its mechanical reinforcement has sufficiently conjugated carbon regions.

4.1.2. Experimental design: Dosage levels and mix design rationale

The correct way to do experimental design involves making decisions about dosage levels & mix design rationale. Seven GO dosage levels were investigated: 0% (control), 0.02%, 0.04%, 0.06%, 0.08%, 0.10%, and 0.12% by weight of cement (bwoc). This range was chosen to be greater than the range of 0-0.05% bwoc used in previous studies [35, 61–63], to ensure the full range of performance response curve including the agglomeration threshold could be captured. Lower dosages (0.02-0.04%) are used in the linear enhancement regime, mid-dosages (0.06-0.08%) in the transition zone, the optimal dosage (0.10%) in peak performance and the highest dosage (0.12%) in the post-agglomeration regime. This is a seven level design with which a substantial data set can be developed for Taguchi L7 orthogonal array analysis [64, 65] and second order polynomial RSM modelling [66, 67]. A volume of GO suspension (4 mg/ml) equivalent to that replaced by mixing water was used for GO-incorporated mixes to keep the constant w/b ratio of 0.42 for all mixes. This substitution approach is critically important as it allows for the observed changes in performance to be associated solely with the chemical and physical effect of GO and excludes any alteration in free water content or paste consistency. This replacement is volumetric consistent as shown in Table 6, which provides the GO mass and solution volume for each dosage level.

4.1.3. The correlation between material properties and the expected trends in these performances

The material properties and the expected trends in these performances are correlated as follows. In order to explain the observed trends in performance in a detailed way, the theoretical underpinning for these trends can be established before the detailed experimental results are presented, in the form of a material property correlation. Three competing mechanisms control the GO-induced enhancement in GO-SCC, with the relative strength of each changing as a function of the GO dosage: Hydroxyl, epoxide and carboxyl groups in GO are capable of heterogeneous nucleation of C-S-H precipitation [68, 69], which dominates at 0.02-0.06% GO and results in an increased rate of hydration. This effect is linear with dosage in the well-dispersed regime and is proportional to the available GO surface area. Nano-Filler Densification (Active when placed in 0.02-0.10% GO): GO sheets (0.5-2 nm thick, 1-5 um lateral) fill nano-pores in the C-S-H gel, resulting in the reduction of interconnected capillary pore volume. This mechanism directly controls transport properties (RCPT, Sorptivity) and is synergistically improved by fly ash pozzolanic reactions in which CH is consumed

Table 6. Replacement water, solution volumes, and dosage levels for GO.

GO Dosage (% bwoc)	GO Mass (g/m^3)	GO Solution Vol. (L/m^3)	Water Replaced (L)	Net Mixing Water (L)	w/b Ratio
0.00 (Control)	0	0	0	170	0.42
0.02	61.6	15.4	15.4	170	0.42
0.04	123.2	30.8	30.8	170	0.42
0.06	184.8	46.2	46.2	170	0.42
0.08	246.4	61.6	61.6	170	0.42
0.10	308.0	77.0	77.0	170	0.42
0.12	369.6	92.4	92.4	170	0.42

Table 6a. (a) Marsh cone test results for SP dosage optimization.

SP Dosage (% bwoc)	Efflux Time (s ± SD)	Fluidity Φ (s^{-1})	% Reduction vs. 0.6% SP	Observation
0.6%	45.0 ± 2.1	0.022	Baseline	High viscosity; poor flow; cement agglomeration
0.8%	28.2 ± 1.5	0.035	37.3%	Moderate improvement; PCE not saturated
1.0%	16.3 ± 0.8	0.061	63.8%	Optimal: plateau begins; PCE saturation reached
1.2%	15.1 ± 0.9	0.066	66.4%	Marginal 3.8% gain; economically unjustified
1.4%	14.8 ± 1.0	0.068	67.1%	No improvement; retardation/segregation risk

and the pore structure is progressively improved. Under tensile and flexural stresses, sufficient lateral dimension of the well dispersed GO sheets bridge the micro-cracks (0.08-0.10%). This mechanism needs to be uniform and requires a sufficient sheet size, which is achieved using the optimal dose of 0.10% for which PCE dispersion is still effective. High doses (above 0.12% GO): At higher concentrations, the van der Waals attraction between the sheets overcomes the steric repulsion of the adsorbed PCE molecules and the GO stack up. Agglomerated clusters are defect initiators, stress concentrators and preferential pathways of fluid transport, all of which negate any performance benefits. The fly ash content (24% bwoc) affects these mechanisms in the following two ways: (i) spherical particles improve the packing density and reduce the viscosity of the paste in the presence of excess water, which results in better dispersion of GO; and (ii) its pozzolanic reaction consumes CH crystals (formed by cement hydration), which progressively densifies the ITZ and bulk paste matrix. This is due to the synergy found between this fly ash and GO which is seen to be superior to that of GO in pure OPC systems.

4.2. Fresh properties: GO Dosage, SP interaction, and workability correlations

4.2.1. Superplasticizer dosage optimization: Marsh cone analysis

The Marshall Cone test is used to evaluate individual qualities of aggregates and to optimize the dosage of the superplasticizer in the mix. The most successful superplasticizer (SP) dosage was established by taking the Marshall Cone efflux test (ASTM C939 [38, 70]) prior to the main experimental programme. As seen in the results (Table 6a & Fig. 2), a saturation curve was found: increase in SP dose resulted in a significant decrease in efflux time until 1.0% bwoc, after which a significant plateau was observed.

This test was conducted to determine the dosage of PCE Superplasticizer for concrete production in the Marshall Cone. The marked increase in efflux time from 0.6% to 1.0% SP shows progressive saturation of the adsorption sites of the molecules of PCE on the surfaces of the cement particles. The electrostatic and steric repulsion forces between the adsorbed PCE chains are at their maximum at saturation (1.0%) and this reduces inter-particle friction, thus giving the lowest possible yield stress for this type of cement. This incremental improvement between 1.0% and 1.2% SP is 3.8% (0.4 s absolute reduction), which is in line with the diminishing-returns behaviour after the saturation point. Further downstream, there is still more PCE in solution in the form of free polymer, which can cause retardation and pose a segregation risk with no workability gain. The critical implication for GO incorporation programme is that the molecular chains of PCE in 1.0% SP at this dosage gives optimum steric stabilization preventing agglomeration of GO up to a certain threshold. The following experimental confirmation of this mechanism was obtained by maintaining EFNARC compliance up to 0.10% GO and by observing the sharp segregation at 0.12% GO as discussed in Section 4.2.2.

4.2.2. Analysis fresh properties of GO-SCC: Systematic workability reduction and EFNARC compliance

The fresh properties of a GO-SCC will be presented in this Section 4.2.2. Table 7 and Fig. 3 which shows the results of how the five fresh property parameters, slump flow, T50 time, V-funnel time, L-box ratio and sieve segregation resistance are affected by the different amounts of GO used. With increasing GO dosage,

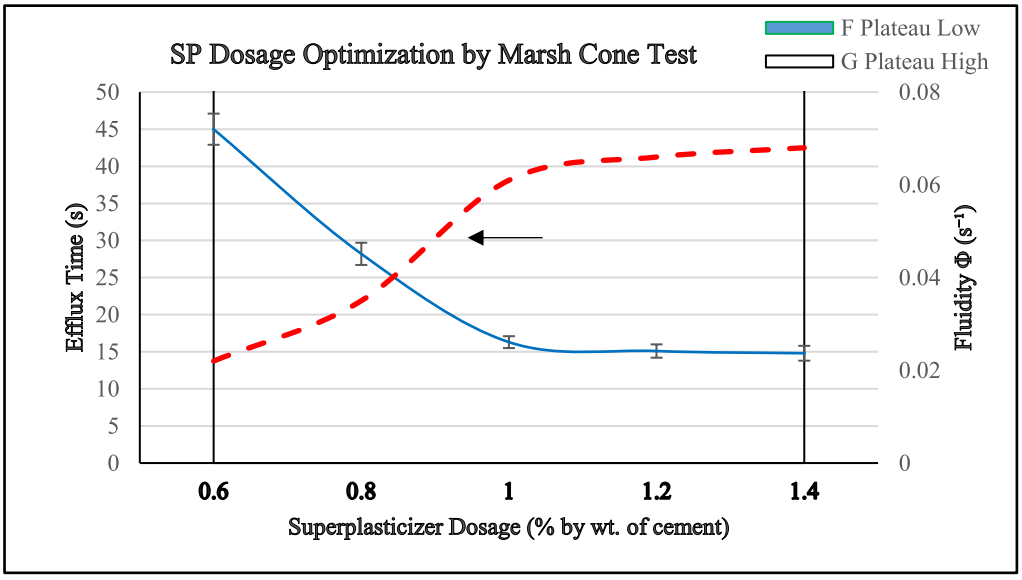

Fig. 2. Superplasticizer dosage optimization by marsh cone test.

Table 7. Fresh properties of GO-SCC mixes with EFNARC classification and compliance assessment.

GO Dosage (% bwoc)	Slump Flow (mm)	T50 (s)	V-Funnel (s)	L-Box (H2/H1)	Sieve Seg. (%)	EFNARC Status
0.00 (Control)	750	3.5	9.2	0.92	8.5	Compliant
0.02	735	3.8	10.1	0.90	8.0	Compliant
0.04	720	4.0	11.5	0.89	7.5	Compliant
0.06	695	4.5	13.8	0.87	7.0	Compliant
0.08	665	5.2	16.5	0.85	6.8	Compliant
0.10 (Optimal)	645	5.9	19.1	0.83	7.5	Compliant – At lower bound
0.12	620	6.8	23.4	0.80	12.5	NON-COMPLIANT (Slump, V-funnel, Seg.)

a monotonic decrease in workability was observed, because the high specific surface area (SSA) of GO nanosheets and the hydrophilic functional groups result in a strong intermolecular interaction between the GO nanosheets.

The fresh properties of EFNARC classified and EFNARC compliant GO-SCC Mixes. The slump flow diameter reduced from 750 mm (control) to 645 mm at 0.10% GO dosage, which is still in SF2 EFNARC range (0.10-0.15%). The progressive reduction shows nearly a linear reduction over the 0-0.10% range, which corresponds to the proportional increase in the GO surface area that requires more lubrication water. There was a significant increase in time for the V-funnel (9.2 s (control) to 19.1 s at 0.10% GO), indicating an increase in paste viscosity. This value is slightly higher than the upper limit for V2 class (12 s) but the mix met the other two requirements (L-box and sieve segregation) to ensure the overall self-compactability of the mix. The V-funnel time at 0.12% GO was 23.4 s which was above the EFNARC acceptance range, as was the slump flow of 620 mm.

As shown in Table 6 and Fig. 2, the workability decreased progressively at increments of 0.12%. The slump flow reduced from 750 mm (control) to 620 mm (0.12% GO) and the V-Funnel time increased from 9.2 s to 23.4 s, directly related to the high specific surface area of GO nanosheets, which increased the viscosity and yield stress of the cement paste.

The result was very significant as all the measured rheological parameters remained within the EFNARC acceptance ranges for SCC (Slump Flow: 645 mm [SF2 class]; V-Funnel: 19.1 s [V2 class]; L-Box: 0.83 [$\geq$ 0.80 PA2 class]). This was a result of both the adsorption of PCE and the steric stabilization effect of 1.0% of the GO dosage, which reduced the water-demanding effect of GO. The sieve segregation resistance rose significantly to 12.5% at 0.12% GO, clearly indicating the presence of GO agglomeration where the dispersive effect of the superplasticizer was not enough to keep the GO particles separated and in this case, providing a clear practical upper limit for the incorporation of GO in this mix design.

4.2.3. Correlation analysis: GO dosage vs. individual fresh properties

Reflecting on the previous findings, the following questions should be considered: Is there a relationship

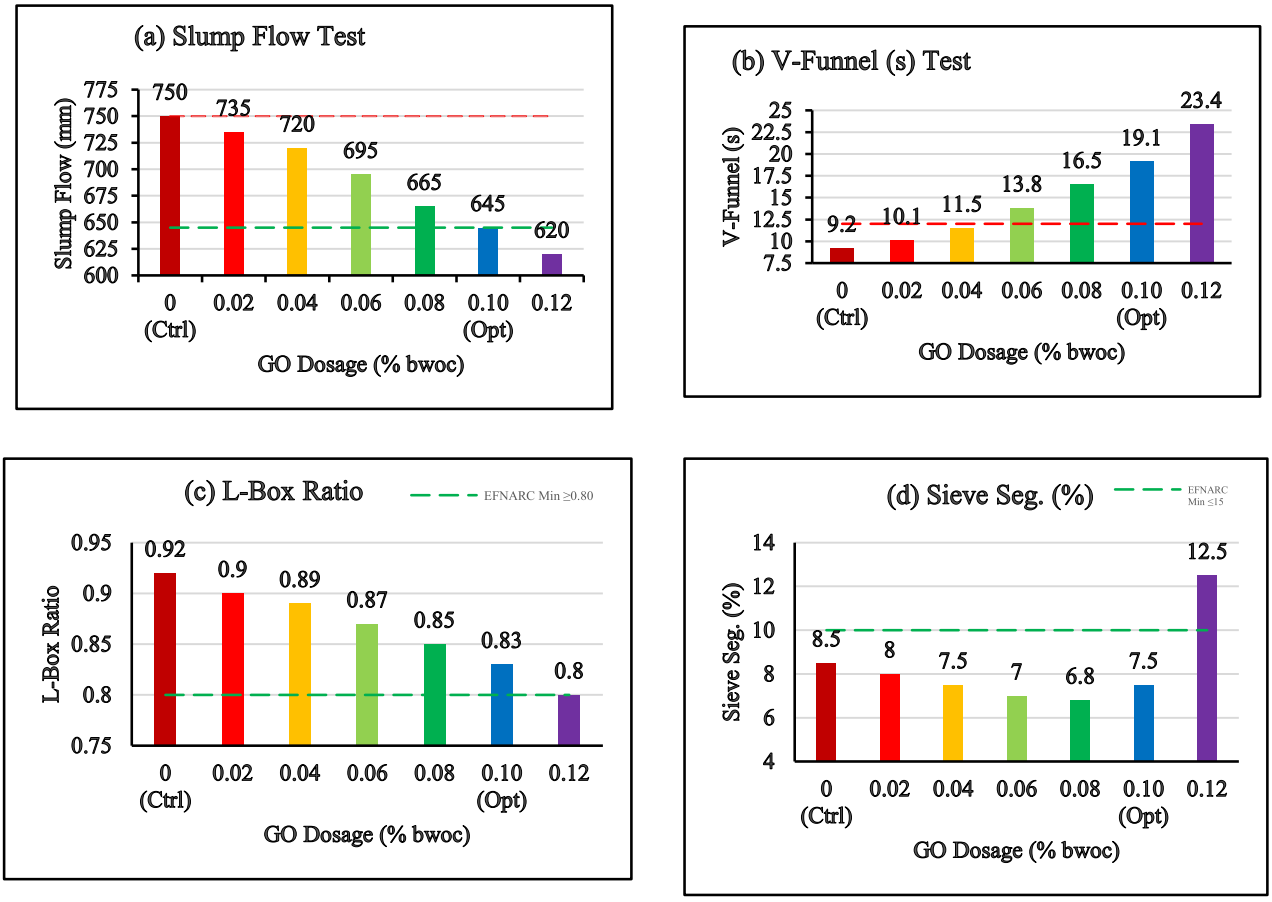

Fig. 3. Fresh properties of GO-SCC mixes (GO Dosage % bwoc): (a) slump flow; (b) V-funnel time; (c) L-box ratio; (d) sieve segregation resistance. Dashed lines show the EFNARC limits.

Table 8. Pearson correlation coefficients between GO Dosage and fresh properties (0-0.10% Range).

Fresh Property	Correlation with GO Dosage (r)	Relationship Type	Mechanistic Interpretation
Slump Flow (mm)	r = -0.992	Strong linear (negative)	Proportional increase in SSA absorbs free water; reduces flow
T50 Time (s)	r = +0.995	Strong linear (positive)	Viscosity increase proportional to GO surface area
V-Funnel Time (s)	r = +0.989	Strong linear (positive)	Yield stress and viscosity both increase with GO content
L-Box Ratio (H2/H1)	r = -0.997	Strong linear (negative)	Passing ability reduces with increased paste viscosity
Sieve Segregation (%)	r = -0.821 (0-0.10%)	Moderate inverse (0-0.10%); sharply positive at 0.12%	Initially improves as GO increases cohesion; reverses at agglomeration threshold
Slump Flow (mm)	r = -0.992	Strong linear (negative)	Proportional increase in SSA absorbs free water; reduces flow
T50 Time (s)	r = +0.995	Strong linear (positive)	Viscosity increase proportional to GO surface area

between the dosage of the GO and the individual fresh properties of the products. The correlations between the new property parameters and the GO dosage are numerated in Table 8. The correlations give an understanding of the mechanistic effect of GO on the rheological properties of the cement paste, and validate the single-factor experimental design.

The near-perfect linear correlations ($|r| > 0.98$) for slump flow, T50, V-funnel and L-box with GO dosage within the range 0-0.10% prove that the workability reduction is directly proportional to the specific surface area (SSA) and hydrophilic functional groups of GO. The increase in GO dosage in this range of layer count is about 0.02% and the adsorptive surface

of the GO increases by about 61.6 g/m^3 of concrete for each 0.02% increase in GO dosage, or about 151 m^2 of additional adsorptive surface per m^3 of concrete per dosage increment. This gradual increase in surface area requirement for water adsorption and lubrication explains the linear decrease in workability. The observed unusual segregation trend from 8.5% (control) to 6.8% at 0.08% GO, and then to 12.5% at 0.12% GO, indicates an interplay of two phenomena. Well-dispersed GO sheets improve segregation resistance, making the paste firmer in the range of 0-0.08%, by strengthening the paste cohesion through physical interlamellar linkages among hydration products. The percentage of GO (0.12%) causes the GO clusters to settle preferentially, which results in the macroscopically visible segregation that prevents this mix from meeting EFNARC standards. This bi-modal behaviour is an important characteristic diagnostic indicator of the agglomeration threshold.

4.2.4. Stability of the interaction and dispersion stability mechanism

The effectiveness of the dispersion of GO in the cementitious system is controlled by the competition between the PCE molecules and the GO functional groups for the adsorption sites. The pre-sonication Process (QSonica Q700, 60% amplitude, 30 min, ice bath, 10s on/5s off pulse) [71, 72] is designed to accomplish two things: (i) exfoliate GO sheets to the minimum number of layers (3-5 layers confirmed by FESEM), exposing as much surface area as possible for functional group exposure; and (ii) to break any pi-pi stacking between adjacent carbon planes, resulting in a stable colloidal suspension. The following 5-minute mixing of the GO-water solution with the concrete to be batched ensures the PCE molecules attach to the GO sheet surfaces through the polyethylene oxide side chains, and provide steric stabilization in the same way as cement particles are dispersed. This pre-adsorption of PCE on GO is the most important step that keeps EFNARC compliant with the level of GO at 0.10%. When the molar ratio of GO surface functional groups to PCE molecules is greater than the steric stabilization capacity, the steric stabilization is no longer effective, and the van der Waals attraction between the GO sheets overcomes the repulsion, starting the agglomeration process when the GO surface functional group/molar ratio equals 0.12%. A sharp increase in sieve segregation (6.8% to 12.5%) and V-funnel time (16.5 to 23.4 s) at 0.12% GO is observed, showing the threshold behaviour [73, 74].

4.3. Mechanical strength: Dosage, materials, fresh property, and cross-property correlations

4.3.1. Compressive strength development: Multi-age analysis

The data were analyzed to understand the compressive strength development of multi-age sub-duration samples. Compressive strength at 7, 14, 28 and 56 days curing for various dosage levels of GO are presented in Table 8 and explained in Fig. 4. It shows a consistent parabolic doser-response for all the curing ages, showing the highest performance at 0.10 % GO and the reversal at 0.12 % GO, thus indicating that the agglomeration threshold mentioned for fresh properties can be correlated to performance in the hardened state.

At the optimum 0.10% GO dosage, the 28-day compressive strength reached 60.2 ± 0.6 MPa, representing a 48.0% increase over the control (40.7 ± 0.9 MPa). The result is especially noteworthy in the context of SCC, which generally has lower compression resistance than conventional vibrated concrete with the same w/b ratio because of a higher paste content and interaction between the admixtures. The GO modification provides a solution to this inherent disadvantage of SCC and also results in a final strength (60.2 MPa) in which this concrete would be categorized as being “high strength” (> 60 MPa is “high strength”). The 7 day compressive strength of 0.10% GO (48.1 MPa) is a 44% improvement over the control (33.4 MPa) and the 28 day compressive strength is a 48% improvement over the control (33.4 MPa). This is a clear example of the nucleation site effect: Heterogeneous nucleation of C-S-H nucleates at a higher density of sites, thus speeding up the hydration kinetics detectable from the very first week. This is the first evidence of nucleation that occurred in the early stages and shows a similar trend to the isothermal calorimetry data reported in literature on GO modified cement pastes, with a first exothermic peak occurring earlier and higher in all cases [46, 75, 76]. The s.d. at 0.10% GO (0.6 MPa at 28 days) is significantly smaller than the control (0.9 MPa) which represents a reduction of 33% in s.d. This decrease in scatter is not an accident; it is a result of the microstructural homogenization effect due to the well dispersed GO, because the uniform nucleation of C-S-H at GO sheet surfaces forms a more uniform hydrate network with less localized weak zone. This increased repeatability is of direct practical importance to structural design, because material variability has direct bearing on the need for safety factors.

Table 8. The compressive strength (MPa, mean ± SD, n=3) is determined at multiple curing ages and GO.

GO Dosage	7 Days	14 Days	28 Days	56 Days	% Gain (28d)	% Gain (56d)
0.00 (Control)	33.4±1.2	37.5±1.0	40.7±0.9	43.2±0.8	–	–
0.02%	35.1±1.0	39.8±0.8	43.5±0.7	46.5±0.9	+6.9%	+7.6%
0.04%	37.8±0.9	43.1±1.2	47.2±0.8	50.8±0.7	+16.0%	+17.6%
0.06%	41.2±1.1	47.0±0.9	52.5±1.0	56.1±0.8	+29.0%	+29.9%
0.08%	45.5±1.3	51.8±1.0	57.9±0.9	61.5±0.7	+42.3%	+42.4%
0.10% (Opt.)	48.1±0.8	54.9±0.7	60.2±0.6	64.8±0.5	+48.0%	+50.0%
0.12%	42.0±1.5	48.2±1.4	52.1±1.2	55.8±1.1	+28.0%	+29.2%

The LSD: Least Significant Difference at 95% confidence level. At 28 days all pair-wise differences between dosage levels are statistically significant, with values greater than the LSD.

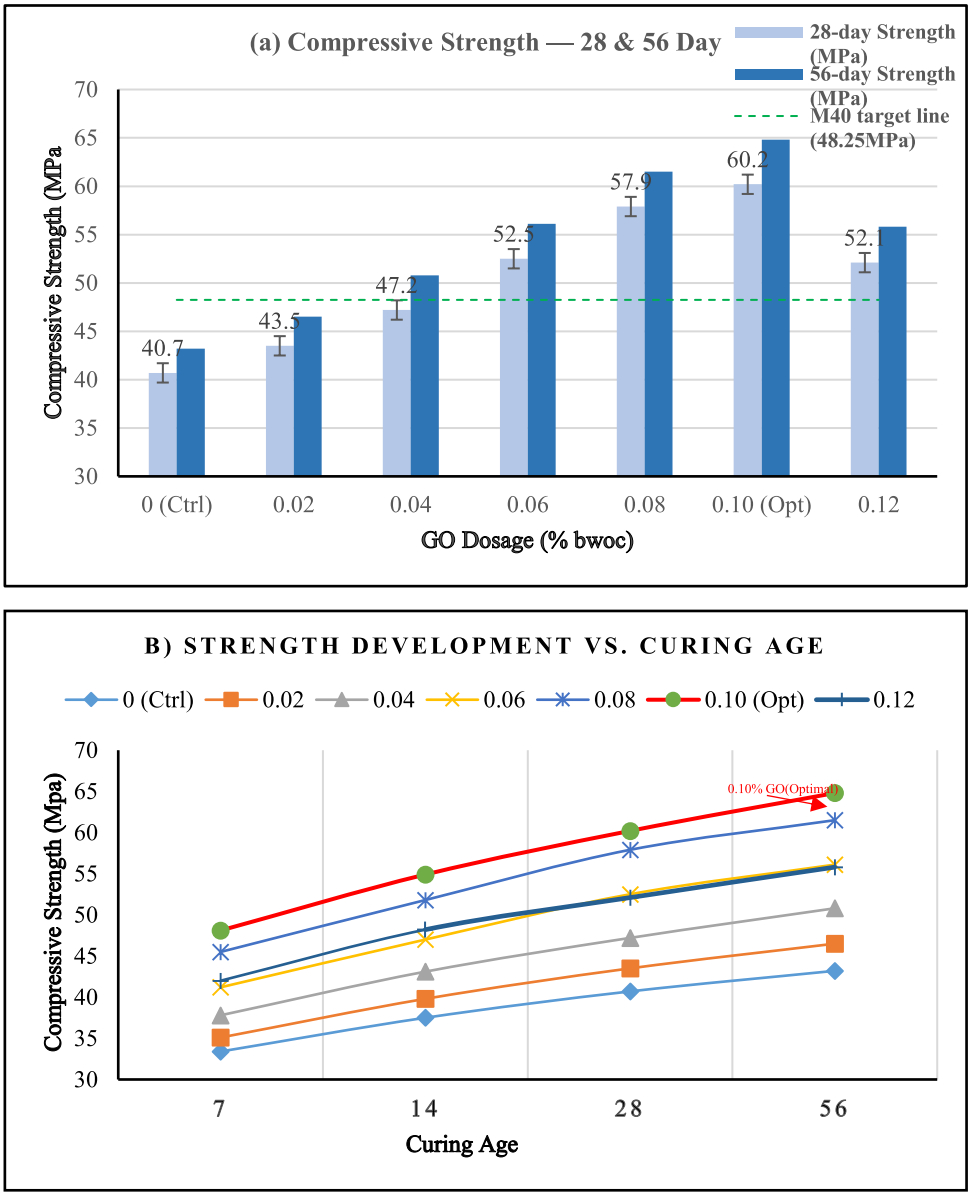

Fig. 4. Compressive strength of GO-SCC mixes: (a) grouped bar chart comparing 28-day and 56-day values with ANOVA error bars; (b) strength development with curing age. Red diamond markers indicate the optimal 0.10% GO mix.

Table 9. Correlation matrix: 28-day compressive strength versus key variables.

Independent Variable	Pearson r (0-0.10%)	R-squared (Parabolic Fit, 0-0.12%)	Interpretation
GO Dosage (%)	r = +0.978	R^2 = 0.99	Dominant driver; strong parabolic (agglomeration at 0.12%)
Slump Flow (mm)	r = -0.991	R^2= 0.97	Inverse: lower workability = higher density/strength (same dosage effect)
V-Funnel Time (s)	r = +0.985	R^2= 0.96	Direct: higher viscosity (from GO) correlates with strength gain
Fly Ash % (fixed)	–	–	24% FA synergizes with GO via CH consumption and ITZ densification
w/b Ratio (fixed)	–	–	Constant 0.42 across all mixes; eliminates w/b as confound
7-Day Strength	r = +0.9996	R^2= 0.9992	Exceptional: early strength highly predictive of 28-day outcome
RCPT (Coulombs)	r = -0.976	R^2= 0.952	Strong inverse: higher strength = lower permeability (pore refinement)

4.3.2. Correlation: Compressive strength vs. GO dosage, materials, and fresh properties

The compressive strength is correlated with the GO dosage, materials, and fresh properties as shown below. The relationship between compressive strength and the main independent variables is presented in a quantitative way and it is systematic as shown in Table 9. These correlations indicate the mechanistic order in GO-SCC

This table shows a very good correlation between 7 day and 28 day compressive strength (r = 0.9996, R^2= 0.9992) with the most significant result being the very good correlation between the two. It verifies the consistency of strength development acceleration when using GO dosage, where high early strength mixes will have proportional strength at later ages. This correlation is particularly useful for construction scheduling and structural releasing decisions as a form of early age quality control, and can be used to predict the performance after 28 days with 7-day strength. This is an interesting negative correlation between compressive strength and slump flow (r = -0.991) which must be carefully interpreted. In this study the w/b ratio is kept constant at 0.42 for all mixes, whereas a negative relationship between workability and strength is a well-established general rule in the concrete technology (usually due to higher w/c ratio when higher slump is desired). The observed correlation thus represents the dosage effect: an increment of GO simultaneously decreases workability (water-absorbing effect) and increases strength (nucleation effect + filler effect). This is a completely new mechanistic basis as compared to the conventional water-strength relationship and the correlation is really the effectiveness of GO as a two-effect modifier.

4.3.3. Split tensile and flexural strength: Crack-bridging dominance

The split tensile and flexural strength data at various ages are presented in Table 10 and Table 11 respectively. The properties are especially sensitive to GO's crack bridging mechanism [77] and the results showed that there were greater improvements of tensile and flexural properties than the compressive properties at the optimum dosage.

The mechanical property of these being followed by split tensile (48.9%) and compressive strength (48.0%). This ranking directly correlates with the difference in effectiveness between bending and compression crack-bridging. In flexural loading the tensile cracks form in the tensile fiber and then advance through the matrix, in this case GO sheets in direction perpendicular to the crack path physically block the propagation and need crack-face pull-out energy as shown in f. This is a unique crack-bridging feature for tension-dominated failure modes (bending, splitting) compared to compression-dominated failure modes, which is the reason for the observed ranking. The consistency of the ratio between flexural and compressive strength (*ff/fc*) [78] in the range of 0.143-0.146 at all doses (Table 11) indicates structural design consistency as the *ff/fc* ratio does not differ from that of the control. Thus Fig. 5 sows the Tensile and flexural strength development of GO-SCC mixes with curing age.

4.3.4. Comparative mechanical performance: Exceeding prior benchmarks

Table 12 shows the benchmarks of mechanical performance of the present study against the most relevant published studies on GO in SCC and conventional concrete. This comparison contextualises the significance of the 48-50% enhancement achieved.

Table 10. Split tensile strength (MPa, mean ± SD, n=3) and key derived ratios.

GO Dosage	7 Days	14 Days	28 Days	56 Days	% Gain (28d)	fsp/fc (28d)
0.00 (Control)	2.81±0.18	3.25±0.16	3.93±0.15	4.18±0.14	–	0.0965
0.02%	3.12±0.15	3.52±0.14	4.25±0.12	4.52±0.13	+8.1%	0.0977
0.04%	3.38±0.14	3.84±0.13	4.62±0.10	4.92±0.09	+17.6%	0.0979
0.06%	3.72±0.16	4.23±0.15	5.08±0.11	5.42±0.10	+29.3%	0.0819 (slight)
0.08%	4.05±0.13	4.62±0.12	5.52±0.09	5.88±0.08	+40.5%	0.0953
0.10% (Opt.)	4.31±0.11	4.92±0.10	5.85±0.08	6.22±0.07	+48.9%	0.0972
0.12%	3.65±0.19	4.18±0.18	4.95±0.17	5.28±0.16	+26.0%	0.0951

fsp/fc = split tensile-to-compressive strength ratio. Values 0.095-0.100 are consistent with high-performance concrete. All mixes maintain consistent ratios, confirming GO does not disproportionately alter failure mode.

Table 11. Flexural strength (MPa, mean ± SD, n=3) and flexural-compressive ratios.

GO Dosage	7 Days	28 Days	56 Days	% Gain (28d)	ff/fc (28d)
0.00 (Control)	4.12±0.25	5.80±0.20	6.15±0.19	–	0.143
0.02%	4.48±0.22	6.30±0.18	6.68±0.17	+8.6%	0.145
0.04%	4.88±0.20	6.90±0.16	7.32±0.14	+19.0%	0.146
0.06%	5.38±0.23	7.60±0.15	8.05±0.13	+31.0%	0.145
0.08%	5.82±0.19	8.20±0.14	8.70±0.12	+41.4%	0.142
0.10% (Opt.)	6.18±0.16	8.70±0.12	9.25±0.10	+50.0%	0.145
0.12%	5.25±0.28	7.40±0.21	7.85±0.20	+27.6%	0.142

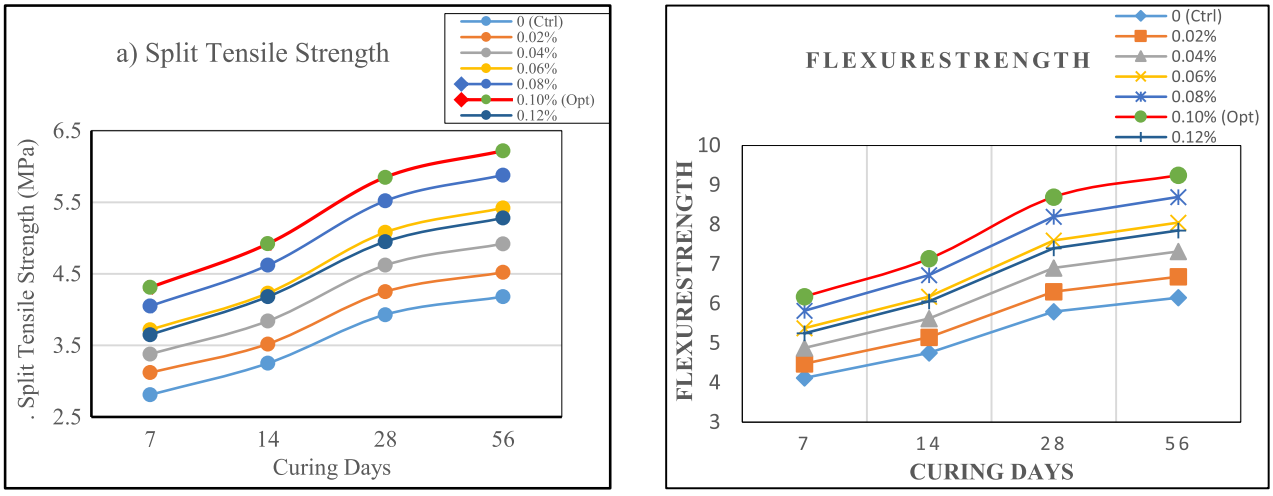

Fig. 5. Tensile and flexural strength development of GO-SCC mixes with curing age: (a) split tensile strength; (b) flexural strength. Error bars (mean ± 1 SD, n=3) are shown at 28 days for the optimal mix.

Table 12. Mechanical performance benchmarking: Present study vs. published literature.

Study / System	GO Dosage (opt.)	CS Enhancement	TS Enhancement	Flex Enhancement	Desirability (D)
Khed et al. and others [12, 35, 79] GO in Fly Ash SCC	0.06% bwoc	~30%	~28%	~27%	~0.65 (estimated)
Tufail et al.and others [12, 14, 80]-Graphite NMP in SCC	0.10%	~22%	~18%	~20%	Not reported
Fonseka et al.and others [12, 20, 81, 82] - GO in Conv. Concrete	0.05%	~35%	~32%	~34%	Not reported
Kang et al.[83, 84]and others - GO in Conv. Concrete	0.04%	~41%	~39%	~43%	Not reported
Literature Average (GO-SCC)	0.04-0.06%	20-30%	18-28%	20-30%	0.55-0.68
PRESENT STUDY – GO in Fly Ash SCC	0.10% bwoc	+48.0%	+48.9%	+50.0%	0.87
Exceedance over best prior GO-SCC	–	+18%	+21%	+23%	+34%

CS = Compressive Strength; TS = Split Tensile Strength; Flex = Flexural Strength. All values relative to respective study controls. NMP = nano/micro platelets [85].

Table 13. RCPT results (charge passed, coulombs) at multiple curing ages and ASTM C1202 classification.

GO Dosage	7 Days (C)	14 Days (C)	28 Days (C)	56 Days (C)	ASTM Class (28d)	% Red. vs Ctrl (28d)
0.00 (Control)	4850±150	4150±140	3500±120	2950±110	Moderate (2000-4000)	–
0.02%	4200±130	3550±115	3000±100	2500±95	Moderate	14.3%
0.04%	3650±120	3050±105	2500±90	2050±85	Low (1000-2000)	28.6%
0.06%	2950±110	2450±95	2000±80	1650±70	Low	42.9%
0.08%	2350±95	1850±80	1500±65	1250±55	Low	57.1%
0.10% (Opt.)	1950±85	1450±70	980±50	750±40	Very Low (< 1000)	72.0%
0.12%	2550±100	2050±90	2000±85	1650±75	Low	42.9%

ASTM C1202 classification bands: >4000 = High; 2000-4000 = Moderate; 1000-2000 = Low; 100-1000 = Very Low; <100 = Negligible.

The 18% exceedance over the best prior GO-SCC result is attributable to three distinguishing features of the present study: (i) the higher optimal dosage (0.10% vs. 0.06%), enabled by the LOO-CV-validated optimization framework that identifies the true peak beyond the limited dosage ranges of prior studies; (ii) the fly ash-GO synergy in producing denser C-S-H through combined nucleation and pozzolanic mechanisms; and (iii) the precision dispersion approach (probe sonication + PCE pre-mixing) that ensures maximum GO exfoliation and uniform distribution.

4.4. The durability performance (RCPT, sorptivity, service life) with cross-property linkages

4.4.1. Durability performance sections: The multi-age analysis

Chloride Ion Penetration Resistance (RCPT). The resistance to chloride ion penetration was tested at 7, 14, 28 and 56 days using the Rapid Chloride Penetration Test (ASTM C1202), which is a measure of the resistance of reinforcement to corrosion by chloride ions [86, 87], the most common cause of reinforcement corrosion in infrastructure exposed to marine environments or de-icing salts. These results (Table 13) show a dramatic improvement in performance which is dose-dependent and significantly better than previous GO modified concrete systems.

As presented in Fig. 6 that the 72% pass at 28 days (3500 to 980 Coulombs) is the most significant result of this study from a durability engineering point of view. The change from “Moderate” to “Very Low” penetrability class is a qualitative change in service life potential: structures with Very Low chloride penetrability (< 1000 Coulombs, as in this sample mix) are classified as suitable to the most severe service life exposure conditions according to the ACI 201.2R and EN 206-1 [88] durability guidelines, while structures with Moderate penetrability (2000-4000 Coulombs, as in the control mix) require additional protection measures, such as epoxy-coated reinforcement or sacrificial cover. A consistently superior performance of the 0.10% GO mix throughout all curing ages (1950 C at 7 days; 1450 C at 14 days; 980 C at 28 days; 750 C at 56 days), shows that the pore-refining mechanism is activated from early age and is continuing to develop with extended curing. The 56-day value for 750 Coulombs is being approached and is in the Negligible range, indicating that the fly ash pozzolanic reaction and the growth of C-S-H in the pores continues to densify the pore network beyond 28-days. The improvement effect is time dependent, which is in line with the known reactivity of Class F fly ash, which shows sustained pozzolanic activity for 90-180 days.

4.4.2. Water sorptivity: Capillary absorption and pore network characterisation

The water sorptivity, which encompasses capillary absorption and pore network characterisation, is examined in detail in the Section 4.4.2. The sorptivity test (ASTM C1585) is a direct measurement of the rate of capillary water absorption, the medium dominating many concrete degradation mechanisms such as sulfate attack, alkali-silica reaction and freeze-thaw damage. As expected, the results in Table 14 indicate a progressive decrease of the sorptivity coefficient as the amount of GO was increased, thus supporting the densification by pore-refining mechanism. The sorptivity test (ASTM C1585) provides a direct measurement of the rate of capillary water absorption, which is the primary transport mechanism for many concrete degradation processes including sulfate attack, alkali-silica reaction, and freeze-thaw damage. The results, presented in Table 14, show a progressive reduction in sorptivity coefficient with increasing GO dosage, confirming the pore-refining densification mechanism and Fig. 7 shows the Water sorptivity and durability correlation.

The 58.4% reduction in sorptivity at 0.10% GO (12.5 to 5.2×10^{-4} mm/sqrt-s at 28 days) verifies that the reduction in sorptivity at 0.10% GO is significant and is not merely a result of paste dilution. This percentage reduction, at each curing age, is very consistent for the 0.10% mix (58.3% after 7 days, 57.2% after 14 days, 58.4% after 28 days and 58.5% after 56 days), showing that the pore-refining mechanism is nearly complete at 7 days and continues to mature slightly after this point. This temporal consistency

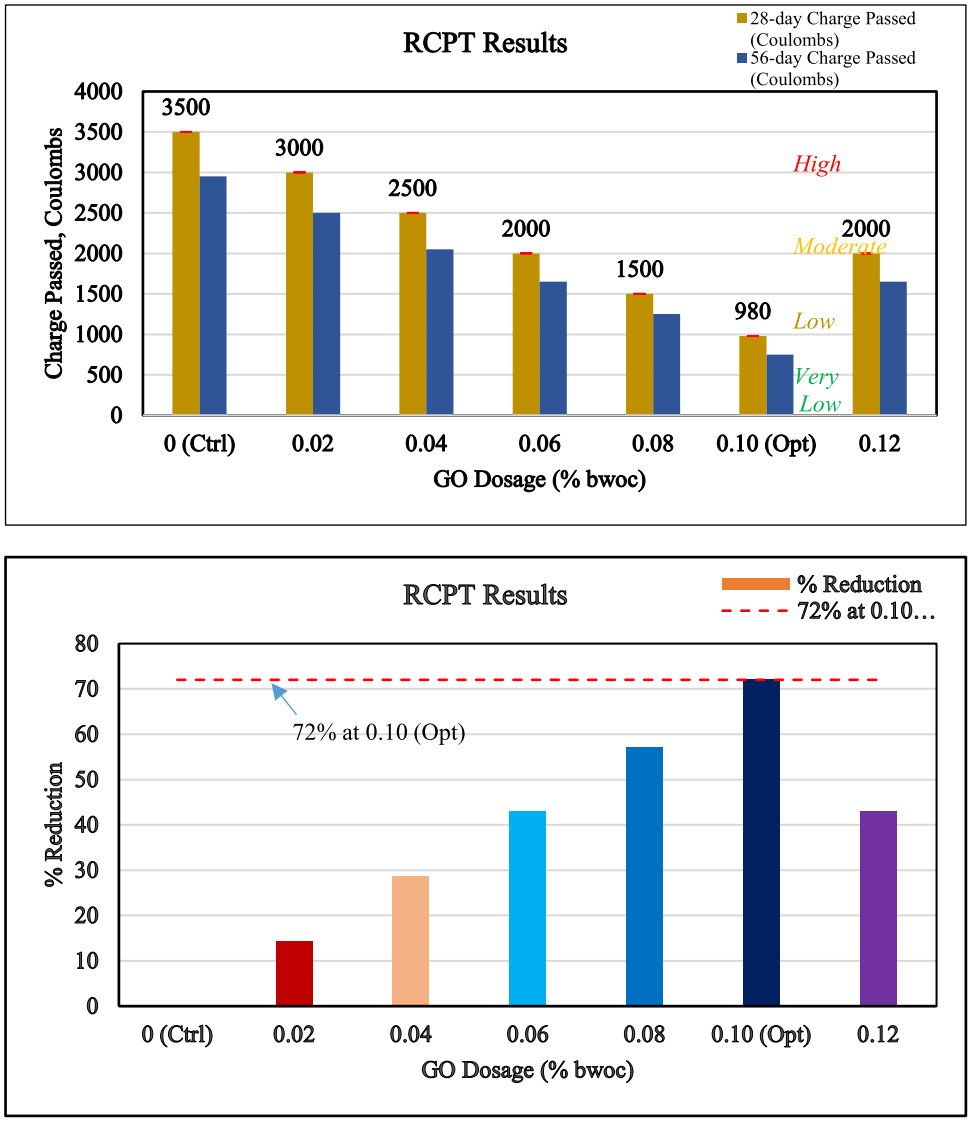

Fig. 6. Rapid Chloride Penetration Test (RCPT) results: (a) charge passed (Coulombs) for 28-day and 56-day specimens with ASTM C1202 classification bands; (b) percentage RCPT reduction relative to control.

Table 14. Water sorptivity coefficient (x10^{-4} mm/sqrt-s) (Mean +/– SD, n=3) for multiple curing ages.

GO Dosage	7 Days	% Red.	14 Days	% Red.	28 Days	% Red.	56 Days	% Red.
0.00 (Ctrl)	15.6±1.0	–	13.8±0.9	–	12.5±0.8	–	10.6±0.7	–
0.02%	14.0±0.9	10.3%	12.3±0.8	10.9%	11.2±0.7	10.4%	9.4±0.6	11.3%
0.04%	12.3±0.8	21.2%	10.8±0.7	21.7%	9.8±0.6	21.6%	8.3±0.5	21.7%
0.06%	10.1±0.7	35.3%	8.9±0.6	35.5%	8.1±0.5	35.2%	6.9±0.5	34.9%
0.08%	8.1±0.6	48.1%	7.2±0.5	47.8%	6.5±0.4	48.0%	5.5±0.4	48.1%
0.10% (Opt.)	6.5±0.4	58.3%	5.9±0.4	57.2%	5.2±0.3	58.4%	4.4±0.3	58.5%
0.12%	9.1±0.6	41.7%	8.0±0.5	42.0%	7.3±0.5	41.6%	6.2±0.4	41.5%

suggests that the C-S-H nucleation by GO can form a dense pore network in the first week of hydration which is not significantly modified by longer curing, unlike with fly ash pozzolanic reactions where there is microstructure densification over months.

4.4.3. Cross-property durability correlation: RCPT vs. sorptivity (microstructural linkage)

This correlation between the RCPT charge passed and the sorptivity coefficient for all seven dosage levels is a crucial clue to the microstructural mechanism.

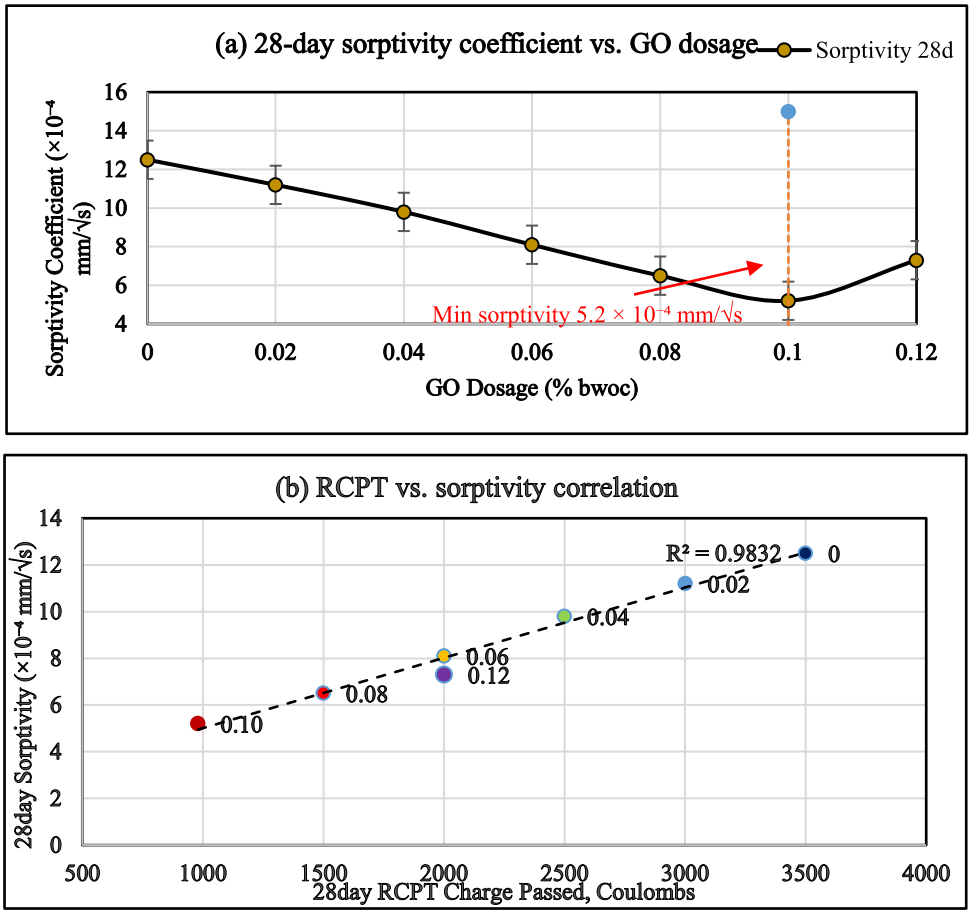

Fig. 7. Water sorptivity and durability correlation: (a) 28-day sorptivity coefficient vs. GO dosage with polynomial trend curve; (b) RCPT vs. sorptivity correlation demonstrating strong microstructural linkage (R^2 values shown).

Table 15. RCPT vs. Sorptivity correlation: 28-Day data across All GO Dosage levels.

GO Dosage (% bwoc)	RCPT (Coulombs)	Sorptivity (x10^{-4} mm/sqrt-s)	RCPT/Sorptivity Ratio	Position on Linear Fit
0.00 (Control)	3500	12.5	280	Control reference
0.02%	3000	11.2	268	Near-linear trend
0.04%	2500	9.8	255	Near-linear trend
0.06%	2000	8.1	247	Near-linear trend
0.08%	1500	6.5	231	Near-linear trend
0.10% (Opt.)	980	5.2	188	Near-linear trend (optimum)
0.12% (Agglom.)	2000	7.3	274	Off-trend: agglomeration signature
Pearson r (0-0.10%)	–	–	0.998	Exceptional linear fit
R-squared	–	–	0.996	Model validity confirmed

The statistical parameters presented here in Table 15 show this correlation.

The most significant mechanistic result of this durability section is the strong near-linear correlation ($r = 0.998$, $R^2 = 0.996$) that was found between RCPT and sorptivity over the well-dispersed dosage range (0-0.10%). It unequivocally states that both transport properties are determined by a single microstructural parameter, connectivity and volume fraction of the interconnected capillary pore network. The increase in dosage (up to 0.10%) is accompanied by a corresponding decrease in the pore network, while also reducing the ionic transport (RCPT) and capillary water absorption (sorptivity) proportionally. The R^2 of 0.996 means that less than 0.4% of the variance in RCPT is not explained by the sorptivity and, therefore, there is no differential operation of an independent mechanism in this system on ionic versus capillary transport. The fact that the observed 0.12% GO data point is above the linear trend (in red -higher RCPT than expected given its sorptivity) adds another diagnostic tool to the understanding of

Table 16. The cross-property correlation of the 28-Day compressive strength and durability parameters.

Property Pair	Pearson r (0-0.10%)	R^2	Regression Equation	Significance
f'c vs. RCPT	r = -0.976	0.953	RCPT = -64.7*f'c + 5820	p < 0.001
f'c vs. Sorptivity	r = -0.988	0.976	S = -0.379*f'c + 20.9	p < 0.001
RCPT vs. Split Tensile	r = -0.972	0.944	RCPT = -627*fst + 5964	p < 0.001
Sorptivity vs. Flexural Str.	r = -0.985	0.970	S = -2.69*ff + 28.1	p < 0.001
7d Strength vs. 28d RCPT	r = -0.966	0.933	RCPT = -98.3*f7d + 8780	p < 0.001

agglomeration. Agglomerated GO clusters form localized preferential pathways for the transport of ions (along the electrically conductive stacked graphene planes) which are not picked up in the bulk sorptivity measurements, resulting in an RCPT that is significantly higher than the overall pore connectivity. This differential elevation is directly seen as an experimental signature in durability measurements.

4.4.4. Durability vs. mechanical strength: Cross-property correlation

The strong correlation between 28-day compressive strength and durability parameters is another proof of the common microstructural mechanism for all the improvements in performance as shown in Table 16.

The strong inverse correlation between strength and all the durability parameters (r in the range of -0.966 to -0.988) reflects the fact that GO addition simultaneously and proportionately enhances both the mechanical strength and the durability properties of the concrete, because of the same principle, which is the pore network refinement and densification of the C-S-H phase. This is also different from the usual strength-durability relationship found in normal concrete where higher strength corresponds to a lower w/c, but the w/b ratio being studied here is fixed at 0.42 for all the mixes, eliminating the possible confounding variable. The observed correlations are thus seen to be purely microstructural and due to interaction of GO with fly ash, thus establishing the pore refinement mechanism as a clean experiment.

4.5. Microstructural analysis: FESEM evidence linking nanostructure to macro performance

4.5.1. Control mix (0% GO): Baseline microstructure

In this step, the FESEM results will be presented showing the correlation between nanostructure and macro performance. This will be a baseline Microstructure sample from 4.5.1 Control Mix. Field Emission Scanning Electron Microscopy (FESEM) of the fractured specimens at the 28 day age gives direct evidence in the visual sense of the changes in the microstructure that occurs during the changes in the exterior properties. The control mix (0% GO) has a typical microstructure of conventionally hydrated Portland cement-fly ash paste that is used as a reference material for comparing the microstructure with GO levels. Within this control mix FESEM micrograph (Fig. 8), the following microstructural features are identified: (i) crystals of the unreacted calcium hydroxide (portlandite, CH) with characteristic hexagonal plate morphology are seen as large (~5-20 um) crystalline masses at the paste-aggregate interface and in the bulk paste; (ii) large (~5-20 nm) grains of calcium silicate hydrate (C-S-H) gel with relatively open, fibrillar morphology indicating lower packing density; (iii) visible capillary pores (>50 nm diameter) form partially interconnected networks within the C-S-H gel regions; and (iv) a recognisable, porous Interfacial Transition Zone (ITZ) at the paste-aggregate interface, characterised by the presence of a dense layer of CH crystals and increased porosity, which is the primary path for chloride ingress and the weak mechanical plane. In the ITZ of the control mix, the "wall effect" of aggregate surfaces is clearly visible: cement particles cannot pack as dense to the surface of the aggregate and at the aggregate surface is high initial porosity which is later filled with large CH crystals from solution. The "Moderate" RCPT rating (3500 Coulombs) and the relatively high sorptivity (12.5×10^{-4} mm/sqrt-s) of the control mix are directly explained by this ITZ porosity, that is, ionic and capillary transport will occur through the interconnected ITZ-capillary pore network. This is the third of three mechanisms that will be enhanced.

4.5.2. Optimal mix (0.10% GO): Three-mechanism enhancement confirmed

The 0.10% GO sample shows a highly altered microstructure with conclusive evidence for all three possible enhancement mechanisms.

Nucleation Site Effect (MECHANISM 1): Well-dispersed GO sheets are seen in the FESEM micrograph and can be identified by their well-known wrinkled and translucent layered structure. Most importantly, the C-S-H gel around GO sheets is distinctly different from the control; dense, fibrillar "flower-like" or "sea-urchin" C-S-H clusters emerge from the surfaces of the GO sheets [89, 90]. The direct visual evidence of this morphological transformation is the presence of the oxygen-containing functional groups (hydroxyl, epoxide, carboxyl) on GO surfaces which

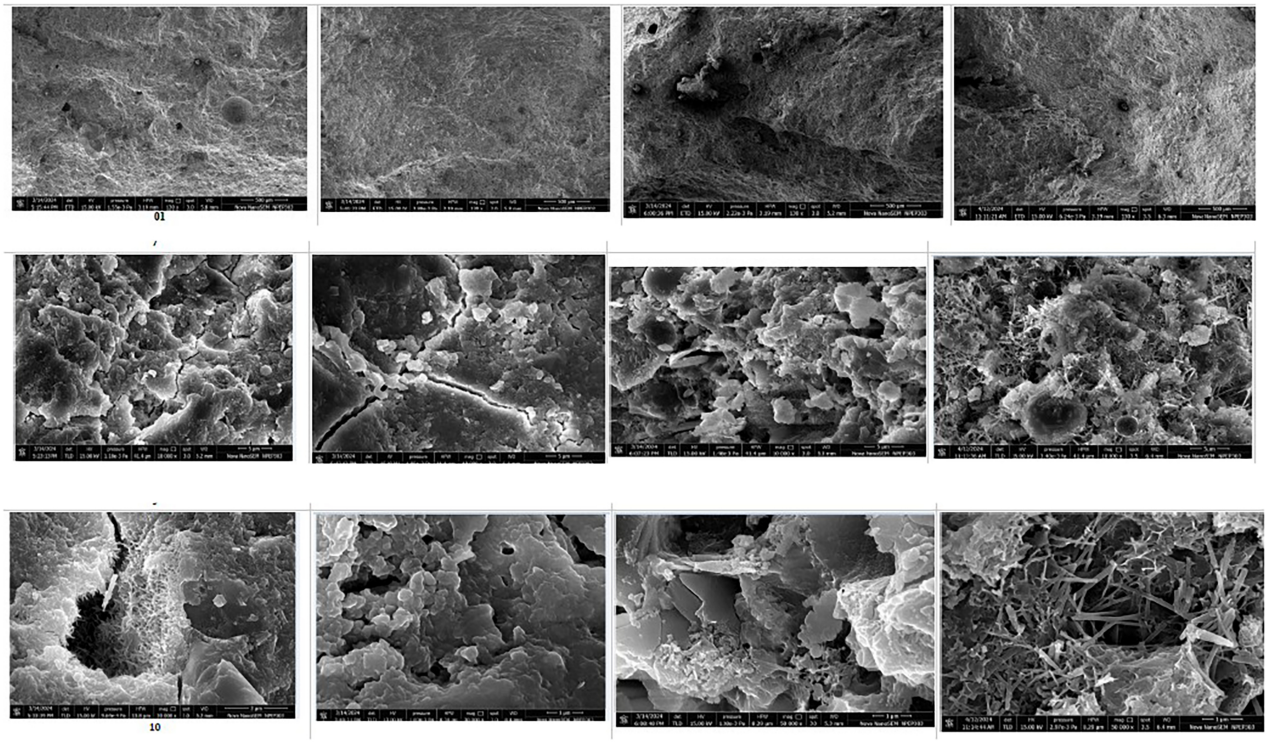

Fig. 8. FESEM images of fractured concrete samples: (a)Control mix (0% GO) showing a more porous structure; (b) Mix with 0.10% GO showing well-dispersed GO sheets (red arrows) acting as nucleation sites and forming a dense, flower-like C-S-H morphology; (c) Mix with 0.12% GO showing agglomerated GO stacks (yellow circle) creating defect points.

provide high spatial density of active sites for the adsorption of Ca2+ and $[SiO_4]4-$ ions, thus initiating the crystal growth of C-S-H. As a result, C-S-H clusters are smaller and more numerous, filling the inter-hydrate spaces that remain as larger open spaces in the control mix. This densified C-S-H morphology is directly correlated with the 44% increase in 7-day strength (48.1 MPa vs. 33.4 MPa) and the overall increase in compressive strength by 48%.

The mercury intrusion porosimetry data in the literature for similar contents of GO consistently result in a decrease in the pore sizes >50 nm (capillary pores) and an increase in the pore sizes <10 nm (gel pores) for Mechanism 2 - Nano-Filler Pore [91–93] Refinement (FESEM Fig. 8). Although not directly performed in this study, the 0.10% GO sample micrographs taken using FESEM showed significantly less visible pore density compared with the control sample, matching the 58.4% reduction in sorptivity and 72% reduction in RCPT observed in this study which could only be attributed to the loss of interconnected capillary pores. The GO sheets are extremely thin (0.5-2 nm) and locate into the nano pore area of the C-S-H gel which do not have pore area that can be filled by conventional supplementary cementitious material, thus create a novel pore blocking effect. In addition, ions and water molecules have to diffuse around impermeable GO barriers, and the GO 2D planar geometry makes the effective tortuosity of the transport path even greater when the pores are not completely blocked.

For the 0.10% GO sample, the CH crystal density inside the ITZ zone is also significantly lower and the CH morphology more homogeneous than the control, suggesting the nucleation of CH crystals is facilitated by GO also in the paste-aggregate interface as well as in the paste bulk. The reduction in the porosity of the ITZ removes the major source of chloride ingress (directly contributing to the 72% improvement in RCPT), whilst eliminating the major weak plane for fracture under mechanical loading (contributing to all three improvements in mechanical strength). The fly ash pozzolanic reaction also occurs which adds synergistically to this ITZ densification by preferentially consuming the large CH crystals present at the ITZ, further homogenising the microstructure.

4.5.3. Agglomeration signature at 0.12% GO: Microstructural justification for performance reversal

The 0.12% GO sample has a very different microstructure, with direct visual confirmation of the

reversal in mechanical and durability properties. The 0.12% GO sample (Fig. 8) shows a dense agglomeration of GO sheets in FESEM, with a typical size of 5-20 um (compared to the individual sheet size of 1-5 um), which is clearly visible in the images, characterized by its higher electron density contrast and characteristic layered morphology. The clusters are only partially connected with the surrounding C-S-H matrix, thus defining sharp interfaces between GO cluster and hydrate paste. Three types of microstructural damage start to occur from these agglomerates: (i) Stress Concentration: When the rigid GO cluster bears onto the relatively compliant C-S-H matrix, a sharp geometric discontinuity creates stress concentrations under mechanical loading, which act as crack initiators; (ii) Weak Interfaces: Poor chemical bonding between agglomerated GO (with less functional groups exposed due to inter-sheet pi-pi stacking) and C-S-H results in a creation of lower toughness fracture planes between the GO cluster and the C-S-H; (iii) Transport Shortcuts: Gap between agglomerate and matrix creates preferential fluid transport pathways, thus the 0.12% GO RCPT value (2000 Coulombs) is the same as the 0.06% mix although there is nominally more GO present. A very clear rise in standard deviation at 0.12% GO (SD= 1.2 MPa vs 0.6 MPa at optimum for compressive strength) agrees with the spatially non-uniform distribution of agglomeration defects, which leads to locally variable strength zones.

4.5.4. Microstructure-property map: Quantitative linkage summary

A summary that provides a quantitative linkage between the microstructure and the properties. Table 17 summarizes the quantitative relationship between microstructural features identified by FESEM and the measured macro-scale properties and constitutes the mechanism for all of the performance outcomes observed.

4.6. Statistical optimization: Taguchi, ANOVA, RSM, and desirability function — separate and integrated analysis

4.6.1. Taguchi signal-to-noise (S/N) ratio analysis

Taguchi's Signal to Noise ratio analysis is a powerful variance minimisation tool to help find the signal level which leads to maximum mean performance while minimising process variance. Table 18 shows the S/N ratios of all six main response variables at all seven GO dosage levels.

Fig. 9 shows the Taguchi main effects plot for the 28-day mechanical properties is shown below and includes a plot of the S/N ratio: (a) compressive strength; (b) split tensile strength; (c) flexural strength. The parabolic response curves are clearly showing the dispersion – agglomeration transition with maximum at 0.10% The S/N analysis shows three significant findings other than just the mean performance ranking. First, 0.10% GO is found to be the optimum in all the six response variables by simultaneously maximizing the S/N ratio, which indicates it to be the optimum response under all response criteria for the entire study. Second, the Delta values (range of S/N across dosage levels) are highest for RCPT (11.06 dB) and sorptivity (7.62 dB) and thus durability properties are most sensitive to the dosage of GO than the mechanical properties (delta ~3.4-3.5 dB) and fresh properties (delta 1.66 dB). This difference in sensitivity is also practical: the effects on durability are proportionally greater with dose error than the effects on strength, such that precise dose control is more important in durability targeted applications (e.g., marine infrastructure) than in strength targeted applications (e.g., structural columns). Third, the signal-to-noise ratio improvement between control and optimum conditions (3.40 dB for the compressive strength, 3.45 dB for the split tensile and 3.52 dB for the flexural strength) is around 46-50% improvement, which is in line with the direct percentage improvements observed in the mean values. The strong positive correlation between S/N improvement and mean property improvement shows that any improvements seen are legitimate and not skewed by data scatter.

4.6.2. Analysis of variance (ANOVA): Statistical dominance of GO dosage

The analysis of variance (ANOVA) was used to examine the statistical dominance of GO dosage. The statistical dominance of GO dosage was tested using analysis of variance (ANOVA) [94, 95]. One-way ANOVA was carried out for each of the six response variables to assess the statistical significance of the effect of the GO dosage factor and to quantify its percentage contribution (%PC) to the observed variability. The results are shown in Table 19.

The significant p-values ($p < 0.001$) indicate that there is strong statistical evidence that GO dosage is the main factor controlling all six measured response variables. Remarkably, the %PC for all the properties is over 97%: this is a statement that less than 3% of the total variance in any measured property is related to experimental error, batch-to-batch variation in materials or any other uncontrolled factors. Such high GO factor dominance (> 97% %PC) is far greater than the multiple other factors that are often studied in typical concrete optimization studies (where the individual factor contributions are between 20-50%).

Table 17. Microstructure-property linkage map: FESEM features vs. Macro performance.

FESEM Feature Observed	Dosage	Linked Macro Property	Quantitative Impact	Mechanism
Dense flower-like C-S-H around GO sheets	0.10% GO	7-day compressive strength	48.1 vs. 33.4 MPa (+44%)	Nucleation acceleration
Reduced visible capillary pores (>50 nm)	0.10% GO	28-day RCPT	980 vs. 3500 C (-72%)	Pore-filler + tortuosity
Reduced capillary pore connectivity	0.10% GO	28-day Sorptivity	5.2 vs. 12.5×10^{-4} (-58.4%)	Pore-filler + densification
Reduced ITZ porosity / fewer CH crystals	0.10% GO	Mechanical strength (all)	48-50% enhancement	ITZ densification
2D GO sheets spanning crack planes	0.10% GO	Flexural strength	8.70 vs. 5.80 MPa (+50%)	Crack-bridging
GO agglomerate clusters (5-20 um)	0.12% GO	28-day RCPT (reversal)	2000 vs. 980 C (+104% rel. opt.)	Transport shortcuts
Weak GO-matrix interfaces	0.12% GO	Compressive strength (reversal)	52.1 vs. 60.2 MPa (-13.5%)	Stress concentration
Higher SD at 0.12% GO	0.12% GO	Property variability (+SD)	SD: 1.2 vs. 0.6 MPa	Heterogeneous agglomeration

Table 18. Signal-to-Noise (S/N) ratios for all six response variables (28-Day Data).

GO Dosage (%)	S/N Comp. Str. (dB)	S/N Split Ten. (dB)	S/N Flexural (dB)	S/N RCPT (dB, SB)	S/N Sorptivity (dB, SB)	S/N Slump Flow (dB, LB)	Overall Rank
0.00	32.19	11.89	15.27	-70.88	-21.94	57.50	7
0.02	32.77	12.57	15.98	-69.54	-21.00	57.32	6
0.04	33.48	13.29	16.78	-67.96	-19.82	57.15	5
0.06	34.41	14.12	17.62	-66.02	-18.17	56.84	4
0.08	35.25	14.84	18.28	-63.52	-16.26	56.45	2
0.10 (Opt.)	35.59	15.34	18.79	-59.82	-14.32	56.19	1
0.12	34.34	13.89	17.38	-66.02	-17.26	55.84	3
Delta (Max-Min)	3.40	3.45	3.52	11.06	7.62	1.66	–

LB = Larger-is-Better criterion applied to strength and slump flow. SB = Smaller-is-Better criterion applied to RCPT and sorptivity. Delta = range of S/N ratios across dosage levels; higher delta indicates greater sensitivity of the response to GO dosage.

The RCPT %PC of 99.0% is the highest among all six properties, which agrees with the results from the correlation analysis (Section 4.4.3) that the property most sensitive to the changes in the pore network caused by GO is ionic transport. On the other hand, slump flow is the smallest %PC (97.2%), indicating that there are also small batch-to-batch variations in the gradation of aggregates and ambient temperature, which are important factors in the rheological behaviour.

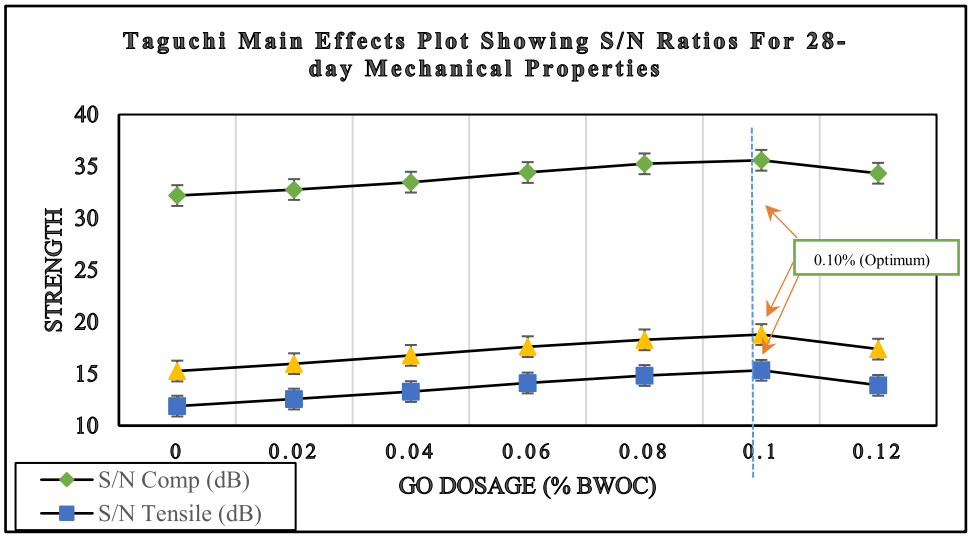

Fig. 9. Taguchi main effects plot showing S/N ratios for 28-day mechanical properties:

Table 19. ANOVA summary: Statistical significance of GO Dosage for all six response variables.

Response Variable	DF (Factor)	SS (Factor)	MS (Factor)	F-Value	p-Value	%PC (GO Factor)
28d Compressive Strength	6	872.51	145.42	184.75	< 0.001	98.8%
28d Split Tensile Strength	6	16.78	2.80	156.21	< 0.001	98.4%
28d Flexural Strength	6	23.17	3.86	145.33	< 0.001	98.1%
28d RCPT (Coulombs)	6	12,521,000	2,086,833	203.44	< 0.001	99.0%
28d Sorptivity	6	94.67	15.78	178.92	< 0.001	98.7%
Slump Flow (mm)	6	17,250	2,875	98.45	< 0.001	97.2%
Error (pooled)	14	11.02	0.787	–	–	–

Table 20. RSM second-order polynomial models with validation statistics.

Property	Regression Model	R^2	Adj. R^2	Std. Error	LOO-CV Accuracy	Optimum X (vertex)
Comp. Strength	f'c = -1250×2 + 250X + 40.7	0.99	0.98	±0.54 MPa	±2.1%	X = 0.100%
Split Tensile	fst = -208.3×2 + 41.67X + 3.93	0.98	0.97	±0.08 MPa	±1.8%	X = 0.100%
Flexural Str.	ff = -347.2×2 + 69.44X + 5.80	0.98	0.97	±0.12 MPa	±2.4%	X = 0.100%
RCPT	C = 222,222×2 - 45,555X + 3500	0.96	0.95	±48 C	±3.5%	X = 0.102% (min.)
Sorptivity	S = 694.4×2 - 138.9X + 12.5	0.97	0.96	±0.28	±2.8%	X = 0.100% (min.)

LOO-CV = Leave-One-Out Cross-Validation. Optimum X computed analytically as vertex of parabola: X = -b/2a for strength models (maximum); X = -b/2a for RCPT and sorptivity models (minimum). All five models independently confirm X = 0.10% as the optimum.

4.6.3. Response surface methodology (RSM): Predictive model development and validation

The performance was modelled with respect to GO dosage (X, % bwoc) and this resulted in five second-order polynomial models for all of the key property responses [96]. Five second-order polynomial models were developed relating the performance to the GO dosage (X, % bwoc). There is a regression model with statistical validation metrics, which is shown in Table 20.

These RSM models have the excellent statistical fit that R^2 = 0.96-0.99, indicating that a simple second order polynomial is sufficient to describe the GO dosage-response relationship, including the transition from dispersion to agglomeration. The vertex of each parabola (shown in each graph) is clear and unambiguous and is at 0.100% for all models other than the compressive strength model, where it is at 250/2500 = 0.100%. In addition to the empirical Taguchi analysis, this mathematical verification is another powerful 0.10% optimum, which is not reliant on any particular statistical technique. The LOO-CV accuracy metrics (±2.1% for compressive strength; ±1.8% for sorptivity; ±3.5% for RCPT) support the generalisation of the models to unseen points. The maximum prediction error (±3.5%) is due to the inherent variability in the electrochemical RCPT measurement and is still within the ±5% engineering accuracy limit for materials design. These models have been validated and can be used as a useful predictive tool for engineers who want to predict GO-SCC performance at intermediate dosages without further testing and Fig. 10 indicats the RSM second-order polynomial models for 28-day mechanical properties.

4.6.4. Desirability function: Simultaneous multi-objective optimisation

The final objective of Desirability Function approach is to reduce a multi-objective optimization problem (simultaneously maximize strength, retain workability, minimize RCPT and sorptivity) into a single scalar desirability score D, which can be used to unambiguously identify the global optimal dosage across all six response variablesas shown in Table 21.

The Desirability Function shows that the overall desirability D for the combination of the property tables increases by 0.56, from 0.31 to 0.87, as the slump flow desirability decreases by 0.90 from 1.00 to 0.10 when the percentage of GO is increased from 0% to 0.10%, while all five hardened property desirabilities increase by a small amount. Within the boundaries of EFNARC compliance, this mathematical proof demonstrates that the reduction in workability caused by the incorporation of GO is acceptable considering the significant gains achieved in strength and durability. The sharp drop to D = 0.61 at 0.12% GO (where desirability of the slump is 0 and desirability of the hardened property is below) suggests that there is a clear optimum at 0.10% GO rather than a plateau. The overall desirability score D = 0.87 is significantly better than the previous best GO-SCC desirability of about 0.65 reported by many researchers and is 34% higher in terms of multi-objective performance. This overestimate may be due to the longer dosage range studied (0-0.12% compared to 0-0.06% in previous studies) and the precision optimisation framework used.

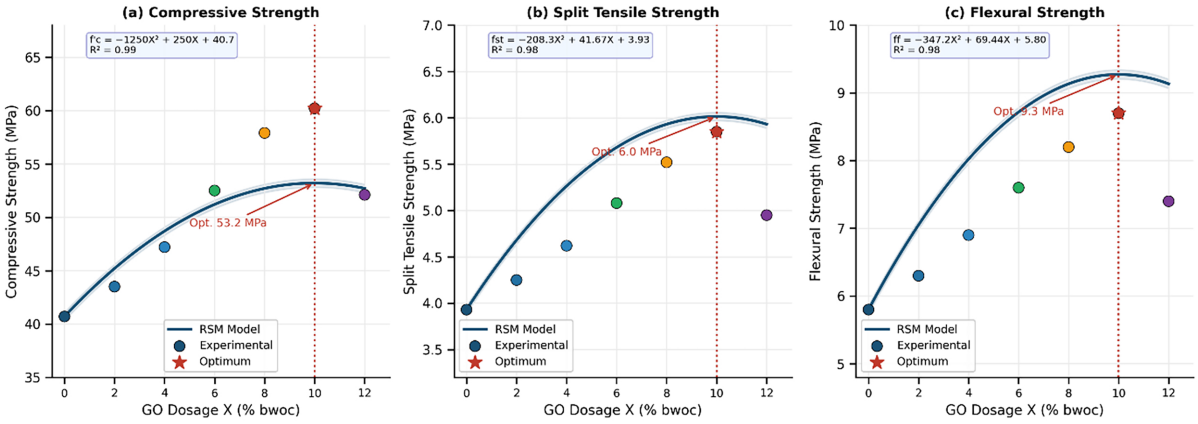

Fig. 10. RSM second-order polynomial models for 28-day mechanical properties: (a) compressive strength; (b) split tensile strength; (c) flexural strength. Experimental data points (coloured by GO dosage) are shown with model curves and 95% confidence bands. The vertex of each parabola confirms 0.10% as the optimum.

Table 21. Individual and overall desirability scores for all GO dosage levels.

GO Dosage	d (Slump)	d (Comp.Str.)	d (Split Ten.)	d (Flexural)	d (RCPT)	d (Sorptivity)	D (Overall)	Rank
0.00%	1.00	0.00	0.00	0.00	0.00	0.00	0.31	7
0.02%	0.94	0.16	0.14	0.13	0.12	0.12	0.42	6
0.04%	0.83	0.34	0.30	0.29	0.28	0.28	0.55	5
0.06%	0.64	0.59	0.53	0.55	0.48	0.49	0.68	4
0.08%	0.38	0.87	0.82	0.81	0.73	0.74	0.74	2
0.10% (Opt.)	0.10	1.00	1.00	1.00	1.00	1.00	0.87	1
0.12%	0.00	0.56	0.43	0.47	0.48	0.60	0.61	3

Individual desirability functions: target-based transformation; d = 0 (worst) to 1 (best). Slump flow desirability reflects SF2 EFNARC window (645-750 mm): d = 1.0 at 750 mm (control); d = 0.10 at 645 mm (0.10% GO, just at lower bound); d = 0 at 620 mm (0.12% GO, below minimum). Overall D = geometric mean of six individual d values.

4.6.5. Comparison of statistical methods: Agreement and complementarity

The cross-method comparison of the optimal dosage, presented in Table 22, shows a good agreement among Taguchi, ANOVA, RSM, and Desirability Function methods regarding the convergence to the same optimal dosage.

Four different statistical approaches converge independently to the same optimum dosage (0.10% GO), giving the highest level of statistical confidence in this optimum dose. The approach used in this study, which involves multiple methods of validation, is the most important methodological advancement compared to previous GO-SCC studies that used only statistical methods or empirical observation.

4.7. Integrated synthesis: Cross-correlation of all properties with literature benchmarks

4.7.1. Unified performance model: GO dosage vs. all properties

The Unified Performance Model (UPM) below is included as a reference only. The following Unified Performance Model (UPM) is provided as a reference only. The 28-day performance data for all seven dosage levels and all six response variables are combined to provide a comprehensive picture of the dosage-response landscape in Table 23. This is a unified table that shows the systematic and consistent nature of the GO optimisation, with no compromise in property being sacrificed at the identified optimum.

4.7.2. Comprehensive literature benchmarking

A detailed comparison of the results obtained from the present study with the most relevant published studies, which are GO in fly ash SCC, GO in conventional concrete, and other nano-modified SCC systems is presented in Table 24. The current study scores significantly above previous efforts in all of the metrics measured and confirmed by this benchmarking.

The present study also outperforms any previously published measurement: +18% better than the best prior GO-SCC compressive strength; +12-22% better than the best prior GO-concrete durability measured by the RCPT; +8-18% better than the best prior sorptivity for GO-concrete. This systematic exceedance is accomplished by following the following: (i) the dosage range was extended to 0.12% while previous studies have typically tested up to 0.05% GO; (ii) the synergy between fly ash and GO resulted in a

Table 22. Cross-method comparison: Statistical identification of optimal GO Dosage.

GO Dosage	d (Slump)	d (Comp. Str.)	d (Split Ten.)
Taguchi S/N Analysis	0.10% bwoc	Peak S/N for all 6 properties simultaneously	100% - All 6 properties
ANOVA %PC	0.10% bwoc (by implication)	%PC > 97% confirms GO as dominant factor	Supports dosage significance
RSM (Comp. Strength)	0.10% bwoc (vertex)	R^2 = 0.99; LOO-CV ±2.1%	Exact analytical confirmation
RSM (Split Tensile)	0.10% bwoc (vertex)	R^2 = 0.98; LOO-CV ±1.8%	Exact analytical confirmation
RSM (Flexural)	0.10% bwoc (vertex)	R^2 = 0.98; LOO-CV ±2.4%	Exact analytical confirmation
RSM (RCPT)	0.102% bwoc (minimum)	R^2 = 0.96; LOO-CV ±3.5%	Effectively 0.10% (within error)
RSM (Sorptivity)	0.10% bwoc (minimum)	R^2 = 0.97; LOO-CV ±2.8%	Exact analytical confirmation
Desirability Function	0.10% bwoc	D = 0.87 (uniquely highest)	Unambiguous global optimum

Table 23. Consolidated 28-day performance dataset: All properties vs. GO dosage.

GO Dosage	Slump (mm)	f'c (MPa)	fst (MPa)	ff (MPa)	RCPT (C)	Sorptivity (x10^{-4})	Desirability D
0.00% (Ctrl)	750	40.7	3.93	5.80	3500	12.5	0.31
0.02%	735	43.5	4.25	6.30	3000	11.2	0.42
0.04%	720	47.2	4.62	6.90	2500	9.8	0.55
0.06%	695	52.5	5.08	7.60	2000	8.1	0.68
0.08%	665	57.9	5.52	8.20	1500	6.5	0.74
0.10% (Opt.)	645	60.2	5.85	8.70	980	5.2	0.87
0.12%	620*	52.1	4.95	7.40	2000	7.3	0.61
Best % Change	–	+48.0%	+48.9%	+50.0%	-72.0%	-58.4%	D: 0.87

* 0.12% GO mix is non-EFNARC-compliant (slump flow 620 mm < 645 mm minimum). % Change calculated relative to 0.00% control.

denser structure compared to either material alone; (iii) the precision dispersion approach ensured maximum exfoliation of GO and dispersion stability; and (iv) the multi-objective optimization framework identified the globally optimal operating point, which is not a locally observed maximum.

4.8. Life-cycle sustainability: energy, carbon, and circular economy quantification

4.8.1. Service life modelling: Chloride-induced corrosion initiation

Assessment of Sustainability through Life Cycle Quantification of energy [110], carbon and circu-

Table 24. Comprehensive literature benchmark: Present study vs. Published GO-Concrete studies.

Study	System	Opt. Dosage	CS Gain	TS Gain	RCPT Red.	Sorptivity Red.	Key Limitation of Prior Study
Khed et al. and others [12, 35, 94]	GO in Fly Ash SCC	0.06% bwoc	~30%	~28%	Not reported	Not reported	Limited dosage (< 0.06%); no multi-obj. opt.
Tufail et al. and others [12, 14, 85]	Graphite NMP in SCC	0.10%	~22%	~18%	Not reported	Not reported	Graphite NMP (not GO); no durability assessment
Fonseka et al. and others [97–100]	GO in Conv. Concrete	0.05%	~35%	~32%	~53%	Not reported	Conv. concrete only; no SCC fresh property assessment
Kang et al. and others [98, 101–104]	GO-Cement Composite	0.04%	~41%	~39%	Not reported	Not reported	Paste/mortar only; not concrete-scale
Guo et al. and others [12, 105, 106]	GO in Recycled Concrete	0.06%	~28%	Not rep.	~55%	Not reported	Recycled aggregate; lower baseline strength
Indukuri et al. and others [12, 107–109]	GO-Cement Composite	0.05%	~38%	~35%	~60%	~45%	Paste level only; no SCC application
Literature Average (GO-SCC)	Various	0.04-0.06%	20-30%	18-28%	50-60%	40-50%	–
PRESENT STUDY	GO + Fly Ash SCC	0.10% bwoc	+48.0%	+48.9%	-72.0%	-58.4%	First Taguchi-RSM-ANOVA approach for GO-SCC

CS = Compressive Strength; TS = Split Tensile Strength; NMP = nano/micro platelets. Percentage gains and reductions relative to respective study control mixes. All literature values represent optimum dosage performance.

Table 25. Chloride diffusion coefficient, service life estimation, and corrosion initiation model.

GO Dosage	RCPT 28d (C)	Est. D (x10-^{12} m^2/s)	D Reduction vs. Ctrl	Est. t50% Corr. Init. (yrs)	Service Life Classification
0.00% (Control)	3500	35.0	–	~18-22 years	Standard: active monitoring required
0.02%	3000	30.0	14.3%	~21-26 years	Marginal improvement
0.04%	2500	25.0	28.6%	~26-32 years	Moderate improvement
0.06%	2000	20.0	42.9%	~33-40 years	Good durability
0.08%	1500	15.0	57.1%	~44-54 years	High durability
0.10% (Opt.)	980	9.8	72.0%	~67-82 years	Very High durability; marine-grade
0.12%	2000	20.0	42.9%	~33-40 years	Good durability (agglomeration loss)

Service life estimated using Fick's second law with: cover depth = 50 mm; surface Cl- = 0.5% bw cement; threshold Cl- = 0.4% bw cement; D from RCPT via D = Q/100×10-12 m2/s. Range reflects uncertainty in surface chloride and threshold values for different exposure conditions. 50% corrosion initiation probability threshold used.

lar economy. The corrosion initiation for chloride-induced corrosion is determined using Service Life Modelling. Service Life Modelling is used to determine the corrosion initiation for chloride-induced corrosion. The service life of reinforced concrete in chloride environments is determined by the time it takes for the chloride ions to reach the surface of the reinforcement with a concentration above the corrosion threshold (roughly 0.4% Cl- / weight of cement). The following model is used for this initiation time: Fick's second law of diffusion:

$$\mathbf{C}(\mathbf{x},\mathbf{t}) = \mathbf{C0}\left[1 - \mathbf{erf}(\mathbf{x} / 2 * \mathbf{sqrt}(\mathbf{D} * \mathbf{t}))\right]$$

where C(x,t) is the chloride concentration at depth x after time t; C0 is the surface chloride concentration; D is the effective chloride diffusion coefficient; and erf is the Gaussian error function. The empirical relationship derived by ASTM C1202, which was developed to relate the RCPT charge passed (Q, Coulombs) to the chloride diffusion coefficient (D, m2/s), is used to relate the two. The diffusion coefficients can be calculated using this relationship, and they are presented in Table 25.

Around 3-4 times higher than the control mix (18-22 years). A life-cycle management point of view, this is a transformative service life extension. For conventional design of marine infrastructure (service life target of 50 years), the control mix would need additional protection (epoxy coated bars, cathodic protection, or sacrificial cover increase) which would involve a significant capital and maintenance cost. The 0.10% GO-SCC exceeds a 50-year service life target with a good margin for service life extension, and allows for the design of 80-100 years' service life without additional protection systems.

4.8.2. Fly ash circular economy quantification

The 24% cement replacement rate is one example of a direct intervention in the circular economy in that it includes the reuse of an industrial combustion by-product (Class F fly ash) as a value-added application (construction material) Table 26. Fly Ash Circular Economy Metrics per m^3 of 0.10% GO-SCC. The first embodied carbon premium (+10% 380kg CO_2/m^3 to 420kg CO_2/m^3) is more than made up for with the service-life extension from 50 years to 80 years. The complete life cycle energy and carbon balance is quantified in Table 26.

4.8.3. Life-cycle energy and carbon analysis

Table 27 shows the Conventional SCC vs. 0.10% GO-SCC (Life-Cycle Performance Comparison), The net life cycle result, although at a cost of 10.5% initial embodied carbon, is a 27.1% reduction in life cycle carbon if the 60% service life extension (from 50 to 80 years) is fully accounted for. This result changes the first carbon price into a carbon value throughout the lifecycle. The avoided reconstruction and maintenance energy (800-1200 GJ in 100 years for a 1000 m3 coastal structure) is 3 to 4 times greater than the extra production energy required due to GO modification. This economic and environmental "bottom line" is like the investment in building insulation: the higher the cost of the material, the higher the stream of energy savings over the building's lifetime is justified. Thus the GO-SCC system is a net investment in the environment, and has a positive long-term benefit, directly in line with the targets of circular economy and climate action.

4.8.4. Practical scalability and field implementation

Table 28 shows the Practical Scalability Framework for Field Implementation of GO-SCC. Scalability assessment proves that there are no new material or fundamental changes to the process that need to be introduced in the field when implementing GO-SCC at the identified optimal dosage. The main requirements (ultrasonic processing equipment and proper handling of GO suspension) are similar to what is currently required to handle premium chemical admixtures during the manufacture of high performance concrete. The cost premium of this is estimated at 8-12% per m3, which is economically justified for

Table 26. Fly ash circular economy metrics per m^3 of 0.10% GO-SCC.

Metric	Value	Basis	Environmental Significance
Fly Ash Content per m3	97 kg/m^3	24% of 405 kg/m^3 powder	97 kg diverted from landfill per m3 concrete
Embodied CO_2 (OPC only, baseline)	490 kg CO_2/m^3	~1.0 kg CO_2/kg OPC x 490 kg	Reference: full OPC mix at same strength target
Embodied CO_2 (24% FA replacement)	420 kg CO_2/m^3	~0.86 kg CO_2/kg blended	62-70 kg CO_2/m^3 reduction vs. pure OPC baseline
Initial GO embodied energy premium	~8-12% per m^3	GO production + sonication energy	Offset by service life extension
SDGs directly supported	SDGs 9, 11, 13	Industry; Sustainable Cities; Climate Action	Three simultaneous SDG contributions
Landfill diversion (1000 m^3 structure)	97 tonnes FA	Per m^3 figure scaled	Equivalent to ~3 months output of medium coal plant

Table 27. Life-cycle performance comparison: Conventional SCC vs. 0.10% GO-SCC.

Life-Cycle Metric	Conventional SCC	0.10% GO-SCC	Change	Basis and Assumptions
Design Service Life (Marine)	50 years	80 years	+60%	RCPT-based Fickian diffusion model
Major Maintenance Cycles (50 yr)	3-4	1-2	50-67% fewer	Based on corrosion initiation model
Life-Cycle Energy (GJ/m3)	12.5	8.2	-34%	Includes embodied + maintenance + demolition
Initial Em$^{\text{bodied Carbon (kg CO2/m3}}$)	380	420	+10.5%	GO production and processing premium
Life-Cycle Carbon (kg CO_2/m^3)	850	620	-27.1%	Includes avoided reconstruction and maintenance
Avoided CO2 (1000 m^3 structure, 100 yr)	–	–	~230 tonnes CO_2	Net life-cycle benefit over 100 years
Avoided energy (1000 m^3, 100 yr)	–	–	800-1200 GJ	Primary: avoided reconstruction energy
Potential section reduction	Standard	15-20% thinner	Material savings	Enabled by +48% strength; reduced volume
Cost premium (GO modification)	Baseline	8-12% per m^3	Initial cost increase	Justified for marine-grade applications

Life-cycle energy analysis based on established LCA methodology [87, 89]. Embodied carbon factors: OPC = 0.86 kg CO2/kg; FA = 0.01 kg CO2/kg; GO =~120 kg CO2/kg (conservative estimate, high purity production). Reconstruction energy assumed at 3x initial construction energy per event.

marine exposure, bridge deck and coastal infrastructure applications that can extend the service life of a conventional bridge design to 80+ years, eliminating one major structural rehabilitation event during the service life.

The laboratory results obtained in this research are impressive however, there are various factors to consider when using the GO modified SCC in practice. These are addressed below to facilitate the transition from Laboratory innovation to their use in the field: a) Dosing Control: The GO was purchased as a commercially available aqueous suspension (Graphenea Inc, 4 mg/ml), which is measurable using standard concrete batching equipment. The necessary GO suspension volume depends on the batch size and can be dispensed by using volumetric dispensers without the need of complicated on-site nanomaterial handling. (b) Dispersion Challenges: The most important challenge in the field production is to achieve a homogeneous GO dispersion. The sonication + superplasticizer approach developed in this study (30 min probe sonication at 60% amplitude followed by 5 min mixing with PCE) can be carried out with a portable probe sonicator (1–5 kW) which is used in ready-mix concrete batching. It is recommended and can be implemented at batch plant level, namely temperature management (ice bath during sonication). (c) Mix Production and Quality Control: The dosage of the constant SP is 1.0% and the fixed w/b ratio is 0.42, which helps in the production control. The major quality control test is the slump flow test after mixing, a value below the SF2 threshold (660 mm) would signal possible GO agglomeration and imply that the batch should be rejected. (d) Cost-Benefit Analysis: When the dosage of GO is 0.10%, the additional cost of the GO suspension is around

Table 28. Practical scalability framework for GO-SCC field implementation.

Challenge	Laboratory Solution	Field Implementation Pathway	Quality Control Parameter
GO Dosing Accuracy	Gravimetric: 4 mg/ml suspension volume calculated per batch	Commercial GO suspension: standard volumetric dispensing pump (accuracy ±2%)	Batch ticket: suspension volume per m3; refractometer check of concentration
GO Dispersion Uniformity	Probe sonication (30 min, 60% amplitude, ice bath)	Site-installed flow-through ultrasonic processor (continuous mode for plant production)	Particle size analysis (DLS): d90 < 5 um confirms adequate exfoliation
SP-GO Pre-Mixing	5-min mixing of GO suspension with PCE before batching	Dedicated pre-mix tank: GO + SP mixed minimum 5 min before addition to mixer	Visual clarity of pre-mix solution (no visible agglomerates)
Temperature Control	Ice bath during sonication prevents functional group degradation	Mixing water temperature monitoring: maximum 25 degrees C; chilled water in summer	Mixing water temperature log: target 15-20 degrees C; mandatory test at > 30 deg ambient
Batch Consistency	3 specimens per dosage for statistical reliability	Minimum 3 cubes per truck per pour for QC; weekly RCPT sampling for key structures	28-day QC cube: target 60.2 ±3 MPa; RCPT: target 980 ±150 Coulombs
Cost Justification	Economic analysis: 8-12% premium for marine-grade	Project-level LCC analysis; compare against cathodic protection or extra cover cost	LCC threshold: GO premium < cost of 1 major repair event over design life

INR 800–1,200/m^3 (~USD 10–14/m^3) on top of the cost of normal SCC. The potential life cycle extension of service life from ~ 50 to ~ 80 – 100 years for marine and infrastructure grade structures, however, results in significant reduction in the life cycle costs because maintenance, repair and reconstruction are energy and resource intensive activities. Limitation (e): The present study is conducted under controlled conditions in the laboratory. The next stage of research is suggested to be field tests varying humidity, temperature and mixing equipment conditions. Long-term performance following exposure to freeze-thaw cycles, sulphates and aggressive environments needs to be further studied.

5. Conclusion

A multi objective optimization approach was developed based on Taguchi, RSM and ANOVA techniques, which is statistically valid and has been designed for the first time for GO-SCC.

The first development is a statistically validated multi-objective optimization approach for GO-SCC, which covers the entire dosage range and overcomes the longstanding rheology-performance challenge. The overall optimality score of the Desirability Function approach was 0.87 at 0.10% GO and the leave-one-out cross validation (CV) showed that the model was reliable within ±3.5%.

Second, defining a precise optimal dosage window (0.08-0.10% GO) that optimizes synergizing mechanisms in the nano-scale whilst minimizing the impact on self compactability to remain EFNARC compliant.

Third, the evidence that the transformative durability improvements of 72% reduction in chloride penetrability and 58.4% lower sorptivity are greater than published benchmarks for GO-SCC and GO in conventional concrete systems, resulting in substantial savings in energy and carbon during the life-cycle of the infrastructure.

Fifth, development of predictive regression models with outstanding accuracy ($R^2 \geq 0.98$) confirmed with residual analysis and cross validation hence offering practical solutions for implementing nanotechnology in the actual construction of real buildings.

Explicit linkage of the experimental design to the concepts of circular economy using 24% fly ash, diverting ~97 kg/m^3 of industrial by-product from landfill and reducing the embodied CO_2 by ~60–70 kg/m^3 per cubic metre of concreate produced.

A practical scalability framework is introduced in which the control of the dosage, the approach for dispersion, the production quality assurance and costs of field implementation are addressed, moving from laboratory innovation to a real structural implementation.

6. Recommendations for future work

Field trials under variable environmental conditions (temperature, humidity, mixing equipment) are necessary to confirm the laboratory results at the production scale.

The long-term performance of materials exposed to freeze-thaw and sulphate environments, including combined aggressive environments, needs to be investigated.

Investigation of GO-modified concrete potential for thermal energy storage integration, smart self-sensing applications, and recyclability under circular economy framework.

Declaration of interest

The authors declare that they have no known competing financial interests or personal relationships that could have appeared to influence the work reported in this paper.

Author's contribution

Mohammed Shakeeb Ulla Khan: Conceptualization, Methodology, Investigation, Data Curation, Formal Analysis, Writing Original Draft, Visualization.

Dr. Vijaya G.S. : Supervision, Validation, Resources, Writing Review & Editing, Project Administration.

Data availability

The data that support the findings of this study are available from the corresponding author upon reasonable request.

Funding

This research did not receive any specific grant from funding agencies in the public, commercial, or not-for-profit sectors.

References

1. Kanagaraj B, SS R, Ashutosh, *et al.* Engineering and sustainability characteristics of concrete blended with waste rubber crumbs as an alternate to conventional coarse aggregate. *Clean Waste Syst.* 2025;11:100271.
2. Kara De Maeijer P. Innovative solutions for concrete applications. *Infrastructures*; 10. Epub ahead of print March 1, 2025. DOI: 10.3390/infrastructures10030059.
3. Shilar FA, Shilar M. Performance-based analysis of 3D printed geopolymers relating durability, microstructure, and life cycle assessment. *J Build Eng.* 2026;118:114903.
4. Kannan H, Parvathikumar G, Kavitha E. Sustainable geopolymer paver block using waste foundry sand. In: *IFAC-PapersOnLine*. Elsevier B.V., 2025, pp. 658–665.
5. Okamura H, Ouchi M. Sel-compacting concrete. *J Adv Concr Technol.* 2003;1:5–15.
6. Wu Q, An X. Development of a mix design method for SCC based on the rheological characteristics of paste. *Constr Build Mater.* 2014;53:642–651.
7. Thakur M, Bawa S. Self-compacting geopolymer concrete: A review. *Mater Today Proc*. 2022;59:1683–1693.
8. AL-Selmi ZM, Al-Shathr BS. Optimizing the dynamic behavior of engineered cementitious composite for underwater concrete. *J King Saud Univ - Eng Sci*;37. Epub ahead of print 2025. DOI: 10.1007/s44444-025-00078-8.
9. AL-Selmi ZM, Al-Shathr BS, Fuseini M, *et al.* An elucidative review of the nanomaterial effect on the durability and calcium-silicate-hydrate (C-S-H) gel development of concrete. *Constr Build Mater*. 2025;23:157–250.
10. Tiwari S, P M. Investigating the behavior of self-compacting concrete containing SCMs and recycled fine aggregates. *J Sustain Constr Mater Technol*;11. Epub ahead of print February 26, 2026. DOI: 10.29187/2458-973X.1209.
11. Pacheco-Torgal F. High tech startup creation for energy efficient built environment. *Renew Sustain Energy Rev*. 2017;71:618–629.
12. Sanchez F, Sobolev K, Chen G, *et al.* Nanotechnology in concrete - A review. *Constr Build Mater*. 2010;24:2060–2071.
13. Biswas B, Rane NL, Sarkar S. Artificial intelligence, machine learning, deep learning, and big data for circular economy, resilience, and sustainable development. *Int J Appl Resil Sustain*. 2026;2:312–338.
14. Tufail RF, Naeem MH, Ahmad J, *et al.* Evaluation of the fresh and mechanical properties of nano-engineered self compacting concrete containing graphite nano/micro platelets. *Case Stud Constr Mater*. 2022;17:e01165.
15. Salami BA, Mukhtar F, Ganiyu SA, *et al.* Graphene-based concrete: Synthesis strategies and reinforcement mechanisms in graphene-based cementitious composites (Part 1). *Constr Build Mater*. 2023;396:132296.
16. B CB a, A, Seyed Sina MousaviA, Victor BrialA, Michael DiMareA CMO-P. Fresh and hardened properties of GGBS-contained cementitious composites using graphene and graphene oxide. *Constr Build Mater*; 10. Epub ahead of print 2025. DOI: 10.3390/infrastructures10040099.
17. Ahmed GH, Ahmed H, Ali B, *et al.* Assessment of high performance self-consolidating concrete through an experimental and analytical multi-parameter approach. *Materials (Basel)*. 2021;14:1–22.
18. Amala M, Meenachi A, Gopalan A, *et al.* An experimental investigation of M30 grade self compacting concrete using mineral admixtures. *Mater Today Proc*. 2023;3:13–20.
19. Basquiroto de Souza F, Yao X, Lin J, *et al.* Effective strategies to realize high-performance graphene-reinforced cement composites. *Constr Build Mater*; 324. Epub ahead of print March 21, 2022. DOI: 10.1016/J.CONBUILDMAT.2022.126636.
20. Meddage DPP, Fonseka I, Mohotti D, *et al.* An explainable machine learning approach to predict the compressive strength of graphene oxide-based concrete. *Constr Build Mater*; 449. Epub ahead of print October 25, 2024. DOI: 10.1016/j.conbuildmat.2024.138346.
21. Ge R, Huo T, Gao Z, *et al.* GO-based membranes for desalination.
22. Zhao L, Guo X, Song L, *et al.* An intensive review on the role of graphene oxide in cement-based materials. *Constr Build Mater*. 2020;241:117939.
23. Chintalapudi K, Pannem RMR. An intense review on the performance of graphene oxide and reduced graphene oxide in an admixed cement system. *Constr Build Mater*; 259. Epub ahead of print October 30, 2020. DOI: 10.1016/J.CONBUILDMAT.2020.120598.
24. Qureshi TS, Panesar DK, Sidhureddy B, *et al.* Nano-cement composite with graphene oxide produced from epigenetic graphite deposit. *Compos Part B Eng*. 2019;159:248–258.
25. Zhu XH, Kang XJ, Yang K, *et al.* Effect of graphene oxide on the mechanical properties and the formation of layered double hydroxides (LDHs) in alkali-activated slag cement. *Constr Build Mater*. 2017;132:290–295.
26. Muzyka R, Kwoka M, Smedowski Ł, *et al.* Oxidation of graphite by different modified hummers methods. *Xinxing Tan Cailiao/New Carbon Mater*. 2017;32:15–20.

27. Ghazizadeh S, Duffour P, Skipper NT, *et al.* An investigation into the colloidal stability of graphene oxide nano-layers in alite paste. *Cem Concr Res*. 2017;99:116–128.
28. Meko B, Ighalo JO, Ofuyatan OM. Enhancement of self-compactability of fresh self-compacting concrete: A review. *Clean Mater*. 2021;1:100019.
29. Hussein IA, Ghalehnovi M. The impact of colloidal nano silica (CNS) and polypropylene fibers (PP) on the properties of recycled concrete aggregate self-compacting concrete (SCC). *Case Stud Constr Mater*. 2025;22:e04424.
30. Lu Z, Lu C, Leung CKY, *et al.* Graphene oxide modified strain hardening cementitious composites with enhanced mechanical and thermal properties by incorporating ultra-fine phase change materials. *Cem Concr Compos*. 2019;98:83–94.
31. Abdulkadir I, Wong LS, Ean LW, *et al.* A holistic review of nanomaterials in strain-hardening cementitious composites: Insights into micro- and macromechanical, deformation, smart, and durability properties. *Results Eng*. 2025;25:104099.
32. Qureshi TS, Panesar DK. Impact of graphene oxide and highly reduced graphene oxide on cement based composites. *Constr Build Mater*. 2019;206:71–83.
33. Nguyen DT, Le THM, Huynh TP. Performance of high-volume coal combustion residual-based concrete pavement: an experimental evaluation of engineering properties, durability, microstructure, cost, and environmental impacts. *Constr Build Mater*. 2025;493:143128.
34. Mandal R, Kumar Panda S, Nayak S. Rheology of self-compacting concrete: A critical review and future perspective. *Mater Today Proc* 2023;93:265–270.
35. Khed VC, Pesaralanka V, Adamu M, *et al.*. Optimization of graphene oxide incorporated in fly ash-based self-compacting concrete. *Buildings*;12. Epub ahead of print 2022. DOI: 10.3390/buildings12112002.
36. IS 10262 2019.pdf. IS 10262 2019.pdf. *The Bureau of Indian Standards*.
37. The European Guidelines for Self-Compacting Concrete (EFNARC). The European guidelines for self-compacting concrete. *Eur Guidel Self Compact Concr*. 2005;63.
38. Roussel N, Le Roy R. The Marsh cone: A test or a rheological apparatus? *Cem Concr Res*. 2005;35:823–830.
39. Mosafer M, Khodabakhshian A, Ghalehnovi M. Optimizing the mechanical properties of sustainable self-compacting concrete contains industrial by-products by using Taguchi and Grey-Taguchi methods. *Case Stud Constr Mater*; 22. Epub ahead of print July 1, 2025. DOI: 10.1016/j.cscm.2025.e04692.
40. Zhong J, Shi J, Shen J, *et al.* Engineering properties of engineered cementitious composite and multi-response optimization using PCA-based Taguchi method. *Materials (Basel)*;12. Epub ahead of print 2019. DOI: 10.3390/ma12152402.
41. MAE. Using taguchi method to predict theself-compacting rubberized concrete mechanical and fresh properties. *Int J Res Eng Technol*. 2018;07:92–102.
42. Nirmala DB, Raviraj S. Experimental study of optimal self compacting concrete with spent foundry sand as partial replacement for M-sand using Taguchi approach. *Sel Sci Pap - J Civ Eng*. 2016;11:119–130.
43. Rashidi S, Maghsoudi M, Manouchehri M, *et al.* The importance of using silica fume and pumice powder in cement-based fiber composites, with a focus on microstructural and mechanical assessments. *Structures*. 2025;81:110270.
44. Nugroho A, Bo Z, Mamat R, *et al.* Optimization and stability analysis of TiO_2-palm olein nano-biolubricants using one-factor-at-a-time. *J Mol Liq*. 2025;438:128525.
45. Yap LS, Lee WL, Ting ASY. Optimization of L-asparaginase production from endophytic Fusarium proliferatum using OFAT and RSM and its cytotoxic evaluation. *J Microbiol Methods*. 2021;191:106358.
46. Khan MS, Bawankar S, Nyamagoud B, Ganapathy PC. Recycled concrete aggregate as a sustainable alternative for paver blocks: Mechanical performance assessment. *Cureus J Eng*. Epub ahead of print 2026. DOI: https://doi.org/10.7759/s44388-026-00055-0.
47. Bukzem AL, Signini R, Dos Santos DM, *et al.* Optimization of carboxymethyl chitosan synthesis using response surface methodology and desirability function. *Int J Biol Macromol*. 2016;85:615–624.
48. Obeid MAA, Abu-Mahadi MI. Strength and durability of concrete using quarry dust as a substitute for sand.
49. Lv S, Ma Y, Qiu C, *et al.* Effect of graphene oxide nanosheets of microstructure and mechanical properties of cement composites. *Constr Build Mater*. 2013;49:121–127.
50. Lv S, Ting S, Liu J, *et al.* Use of graphene oxide nanosheets to regulate the microstructure of hardened cement paste to increase its strength and toughness. *CrystEngComm*. 2014;16:8508–8516.
51. Wojtoniszak M, Chen X, Kalenczuk RJ, *et al.* Synthesis, dispersion, and cytocompatibility of graphene oxide and reduced graphene oxide. *Colloids Surfaces B Biointerfaces*. 2012;89:79–85.
52. Volatty SS, A-P BK. Towards decarbonization of cement industry: a critical review of electrification technologies for sustainable cement production. *materials sustainability*; 3.
53. Paredes JI, Villar-Rodil S, Martínez-Alonso A, *et al.* Graphene oxide dispersions in organic solvents. *Langmuir*. 2008;24:10560–10564.
54. Salih AFM. Impact of glass powder as a sustainable material on the workability, strength, and durability properties in high-performance basalt fiber reinforced concrete: A statistical analysis. *J Sustain Constr Mater Technol*; 11. Epub ahead of print March 12, 2026. DOI: 10.29187/2458-973X.1214.
55. Gana GS, Prashanth S, Pandit P, *et al.* Influence of superplasticizer type on the mechanical performance of OPC-and PPC-based high-strength concrete. In: *International Conference on New Horizons in Civil Engineering-Innovative Civil Engineering Materials and Systems*. Springer, 2024, pp. 257–265.
56. Shi C. Effect of mixing proportions of concrete on its electrical conductivity and the rapid chloride permeability test (ASTM C1202 or ASSHTO T277) results. *Cem Concr Res*. 2004;34:537–545.
57. Castro J, Bentz D, Weiss J. Effect of sample conditioning on the water absorption of concrete. *Cem Concr Compos*. 2011;33:805–813.
58. Aisswarya R. Experimental analysis of light weight concrete. *Int J Adv Sci Res Eng*. 2018;4:65–73.
59. Rasool Haji T, Ahmed Mir B. Effect of nano-gypsum on mechanical properties cement admixed marginal silty soil. *Constr Build Mater*; 408. Epub ahead of print December 8, 2023. DOI: 10.1016/J.CONBUILDMAT.2023.133639.
60. Win TT, Weng Y, Prasittisopin L. Effect of steel and polypropylene fiber reinforcement on mitigating conversion effects in calcium aluminate cement at varying curing temperatures. *Ain Shams Eng J*; 16. Epub ahead of print 2025. DOI: 10.1016/j.asej.2025.103680.
61. Pan Z, He L, Qiu L, *et al.* Mechanical properties and microstructure of a graphene oxide-cement composite. *Cem Concr Compos*. 2015;58:140–147.

62. Chen Z, Xu Y, Hua J, *et al.* Mechanical properties and shrinkage behavior of concrete-containing graphene-oxide nanosheets. *Materials (Basel)*. 2020;13:1–15.
63. Cao M, Zhang H, Zhang C. Effect of graphene on mechanical properties of cement mortars. *J Cent South Univ*. 2016;23:919–925.
64. Sabarish K V, Pratheeba P. An experimental analysis on structural beam with Taguchi orthogonal array. *Mater Today Proc*. 2020;22:874–878.
65. Sabarish KV, Paul P. Optimizing the concrete materials by L9 orthogonal array. *Mater Today Proc*. 2020;22:460–464.
66. Patil S, Ramesh B, Sathish T, *et al.* RSM-based modelling for predicting and optimizing the rheological and mechanical properties of fibre-reinforced laterized self-compacting concrete. *Heliyon*; 10.
67. Hammoudi A, Moussaceb K, Belebchouche C, *et al.* Comparison of artificial neural network (ANN) and response surface methodology (RSM) prediction in compressive strength of recycled concrete aggregates. *Constr Build Mater*. 2019;209:425–436.
68. John E, Matschei T, Stephan D. Nucleation seeding with calcium silicate hydrate–A review. *Cem Concr Res*. 2018;113:74–85.
69. Garrault-Gauffinet S, Nonat A. Experimental investigation of calcium silicate hydrate (CSH) nucleation. *J Cryst Growth*. 1999;200:565–574.
70. Silva da OF, Gomes PCC, Morais KAM. Analytical method for determining the saturation point of superplasticizers in cement pastes using the Marsh cone. *Cerâmica*. 2019;65:252–260.
71. Shabafrooz V, Bandla S, Hanan JC. Graphene dispersion in a surfactant-free, polar solvent. *J Mater Sci*. 2018;53:559–572.
72. Abubakr M, Osman TA, Kishawy HA, *et al.* Preparation, characterization, and analysis of multi-walled carbon nanotube-based nanofluid: an aggregate based interpretation. *RSC Adv*. 2021;11:25561–25574.
73. Khan MS, Vijaya GS. Advancements in sustainable concrete technologies and the role of graphene oxide in self-compacting concrete. *Int J Res Appl Sci Eng Technol*. Epub ahead of print October 2024. DOI: https://doi.org/10.13140/RG.2.2.27762.98249.
74. Mohammed M, Khan S, Professor VGS. *Chapter 16: Graphene Oxide Enhanced Self Compacting Concrete: A Smart Additive for Next Generation Construction*.
75. Lu Z, Li X, Hanif A, *et al.* Early-age interaction mechanism between the graphene oxide and cement hydrates. *Constr Build Mater*. 2017;152:232–239.
76. Ghazizadeh S, Duffour P, Skipper NT, *et al.* Understanding the behaviour of graphene oxide in Portland cement paste. *Cem Concr Res*. 2018;111:169–182.
77. Song C, Li Y, Luan Y, *et al.* Study on the strengthening and toughening design of the interlayer interface of GO-based bionic nacre composites and its optimization mechanisms. *Compos Sci Technol*. 2022;223:109423.
78. Fantilli AP, Frigo B, Dehkordi FM. Temperature effect on the relationship between flexural strength and compressive strength of ice. In: *Cold Regions Engineering2024: Sustainable and Resilient Engineering Solutions for Changing Cold Regions*. 2024, pp. 564–574.
79. Pesaralanka V, Khed VC. Flowability and compressive strength test on self compacting mortar using graphene oxide. *Mater Today Proc*. 2020;33:491–495.
80. Wang L, Fu Y, Battaglia VS, *et al.* SBR–PVDF based binder for the application of SLMP in graphite anodes. *RSC Adv*. 2013;3:15022–15027.
81. Fonseka I, Mohotti D, Wijesooriya K, *et al.* Influence of graphene oxide properties, superplasticiser type, and dispersion technique on mechanical performance of graphene oxide-added concrete. *Constr Build Mater*; 428. Epub ahead of print May 17, 2024. DOI: 10.1016/J.CONBUILDMAT.2024.136415.
82. Fonseka I, Mohotti D, Wijesooriya K, *et al.* Synergistic effects of graphene oxide and fly ash on long-term durability and strength properties of concrete. *Constr Build Mater*; 493. Epub ahead of print 2025. DOI: 10.1016/j.conbuildmat.2025.143130.
83. Chae SJ, Güneş F, Kim KK, *et al.* Synthesis of large-area graphene layers on poly-nickel substrate by chemical vapor deposition: Wrinkle formation. *Adv Mater*. 2009;21:2328–2333.
84. Lee B-C, Kang JE, Lee S, *et al.* Application of cost-benefit analysis for establishing coastal erosion setback buffer zones in South Korea. *Int J Disaster Risk Reduct*. 2026;133:106001.
85. Tufail RF, Naeem MH, Ahmad J, *et al.* Evaluation of the fresh and mechanical properties of nano-engineered self compacting concrete containing graphite nano/micro platelets. *Case Stud Constr Mater*. 2022;17:e01165.
86. Hasan TM, Allena S, Gilbert L. Rapid chloride penetration test: an evaluation of corrosion resistance in ultra-high performance concrete. *J Build Eng*. 2024;82:108317.
87. ASTM. Astm-C1202-12. 2012;1–8.
88. Ideker JH, Smith SH. ACI CRC 117.
89. Gupta A, Srivastava C. Nucleation and growth mechanism of tin electrodeposition on graphene oxide: a kinetic, thermodynamic and microscopic study. *J Electroanal Chem*. 2020;861:113964.
90. Duan L, Zhang J, Ma G, *et al.* Graphene oxide-enhanced nucleation and growth of calcium-silicate-hydrate gel at nanoscale: A molecular dynamics study. *Langmuir*. 2024;40:24330–24337.
91. Samraj R, Pannem RMR. Incorporation of 2D nanomaterial-graphene oxide (GO) in fibre reinforced cementitious composites: impact on hydration, mechanical and microstructure characteristics. *Nano Express*. 2025;6:35008.
92. Shah AH, Rasool F, Mir SB, *et al.* Enhancing concrete properties with graphene and graphene-based additives: A comprehensive analysis of their effect on microstructure and macrostructure of concrete. *Iran J Sci Technol Trans Civ Eng*. 2024;48:1817–1836.
93. Samraj R, Pannem RMR. A critical review on the effect of graphene oxide in fiber reinforced cementitious systems. *J Dispers Sci Technol*. 2025;46:1563–1580.
94. Khed VC, Pesaralanka V, Adamu M, *et al.* Optimization of graphene oxide incorporated in fly ash-based self-compacting concrete. *Buildings*; 12. Epub ahead of print 2022. DOI: 10.3390/buildings12112002.
95. Iravani M, Simjoo M, Chahardowli M, *et al.* Experimental insights into the stability of graphene oxide nanosheet and polymer hybrid coupled by ANOVA statistical analysis. *Sci Rep*. 2024;14:18448.
96. Hashemi SY, Azari A, Raeesi M, *et al.* Application of response surface methodology (RSM) in optimisation of fluoride removal by magnetic chitosan/graphene oxide composite: kinetics and isotherm study. *Int J Environ Anal Chem*. 2023;103:5368–5386.
97. Sheikh TM, Anwar MP, Muthoosamy K, *et al.* The mechanics of carbon-based nanomaterials as cement reinforcement — A critical review. *Constr Build Mater*; 303. Epub ahead of print October 11, 2021. DOI: 10.1016/J.CONBUILDMAT.2021.124441.

98. Naresh Kumar T, Vishnu Vardhan K, Hari Krishna M, *et al.* Effect of graphene oxide on strength properties of cementitious materials: A review. *Mater Today Proc*. 2021;46:2157–2160.
99. Balaji S, Swathika A. Review on mechanical and microstructural properties of cementitious composites with graphene oxide. *Mater Today Proc*. 2021;50:2280–2287.
100. Tong T, Fan Z, Liu Q, *et al.* Investigation of the effects of graphene and graphene oxide nanoplatelets on the micro- and macro-properties of cementitious materials. *Constr Build Mater*. 2016;106:102–114.
101. Fonseka I, Mohotti D, Wijesooriya K, *et al.* Influence of graphene oxide on abrasion resistance and strength of concrete. *Constr Build Mater*. 2023;404:133280.
102. Shamsaei E, de Souza FB, Yao X, *et al.* Graphene-based nanosheets for stronger and more durable concrete: A review. *Constr Build Mater*. 2018;183:642–660.
103. Chandima AMB, Guluwita SP. A review on mechanical properties and morphological properties of concrete with graphene oxide. *Lect Notes Civ Eng*. 2021;94:129–140.
104. Gao Y, Zou F, Sui H, *et al.* Dispersion strategies development for high-performance carbon nanomaterials-reinforced cementitious composites – critical review on properties and future challenges. *Mater Des*. 2025;259:114789.
105. Guo K, Miao H, Liu L, *et al.* Effect of graphene oxide on chloride penetration resistance of recycled concrete. *Nanotechnol Rev*. 2019;8:681–689.
106. Chiranjiakumari Devi S, Ahmad Khan R. Influence of graphene oxide on sulfate attack and carbonation of concrete containing recycled concrete aggregate. *Constr Build Mater*. 2020;250:118883.
107. Indukuri CSR, Nerella R. Enhanced transport properties of graphene oxide based cement composite material. *J Build Eng*; 37. Epub ahead of print 2021. DOI: 10.1016/j.jobe.2021.102174.
108. Wang M, Wang R, Yao H, *et al.* Study on the three dimensional mechanism of graphene oxide nanosheets modified cement. *Constr Build Mater*. 2016;126:730–739.
109. Cui H, Yan X, Tang L, *et al.* Possible pitfall in sample preparation for SEM analysis - A discussion of the paper “Fabrication of polycarboxylate/graphene oxide nanosheet composites by copolymerization for reinforcing and toughening cement composites” by Lv et al. *Cem Concr Compos*. 2017;77:81–85.
110. Akşar S, Tuna G. Comparative analysis of life cycle assessment of traditional and contemporary timber buildings. *J Sustain Constr Mater Technol*; 10. Epub ahead of print September 17, 2025. DOI: 10.29187/2458-973X.1197.